Nitrous oxide cycling in the Eastern Tropical South Pacific as inferred from isotopic and isotopomeric data.

Casciotti[1*] K.L., Forbes[1] M., Vedamati[1] J., Peters[1] B., Martin[1] T., Mordy[2,3] C.W.

[1] Department of Earth System Science, Stanford University, 473 Via Ortega, Stanford, California, 94305, USA.

[2] Joint Institute for the Study of the Atmosphere an Ocean, Box 355672, University of Washington, Seattle, WA 98105-5672, USA.

[3] Pacific Marine Environmental Laboratory, NOAA, 7600 Sand Point Way, NE, Seattle WA, 98115, USA.

* Corresponding Author: kcasciotti@stanford.edu, 650-721-5545

Abstract

The ocean accounts for up to 25% of global emissions of nitrous oxide (N_2O), a potent greenhouse gas. Much of this N_2O flux occurs in upwelling regions near the ocean's oxygen deficient zones (ODZs), areas known for intense N_2O cycling. The Eastern Tropical South Pacific (ETSP) ODZ is one such area, and large uncertainties surround the balance of processes regulating N_2O production and emission in this region. Here we examined the distributions of dissolved N_2O concentration and stable isotopic composition, in concert with nitrate (NO_3^-) and nitrite (NO_2^-) isotopic ratios, to understand the mechanisms that drive N_2O production, consumption, and emission from the ETSP ODZ. Keeling plot analysis identified N_2O production from both nitrification and denitrification (or nitrifier-denitrification) in the oxycline, where the largest accumulations of N_2O were found. In the N_2O concentration maximum that occurs below the ODZ, a higher ^{15}N site preference (SP) indicated nitrification was more prominent. Within the ODZ, significant enrichments were apparent in $\delta^{15}N^{bulk}$ (14–22‰), $\delta^{18}O_{N2O}$ (68–100‰) and SP (39–60‰), implying active N_2O consumption. Further scrutiny of N_2O isotope data in the ODZ highlights a deviation from the relative increases in $\delta^{18}O_{N2O}$ and SP expected for bacterial denitrification. At high levels of N_2O consumption, SP increased more than expected for the increase in $\delta^{18}O_{N2O}$. This appeared to be due, at least in part, to a decrease in $\delta^{15}N^{\beta}$ driven by N_2O production in the ODZ, rather than further increases in $\delta^{15}N^{\alpha}$. Isotopic analysis of co-occurring NO_3^- and NO_2^- suggests that NO_3^- may be the dominant source of N_2O in the offshore ETSP ODZ.

1. Introduction

Nitrous oxide (N_2O) is an important greenhouse gas in terms of anthropogenic climate forcing (Myhre et al., 2013), and it plays a critical role in stratospheric ozone depletion (Crutzen, 1970; Ravishankara et al., 2009). Oceanic N_2O production is estimated to contribute up to 25% of total natural and anthropogenic emissions, though there is a great deal of uncertainty in this estimate, especially in coastal areas (Nevison et al., 2004; Bange, 2008; Ciais et al., 2013). Upwelling zones play important roles in oceanic emissions of N_2O (Nevison et al., 2004; Suntharalingam and Sarmiento, 2000; Bange et al., 1996; Kock et al., 2016), and it is estimated that the Peruvian upwelling area alone may supply 0.2–0.9 TgN/yr (Arevalo-Martinez et al., 2015). While increased attention has gone towards understanding the magnitudes and controls on N_2O production and emission from the ocean, significant uncertainties remain that prevent us from making confident projections of future N_2O emissions (Bange et al., 2010; Codispoti, 2010; Zamora et al., 2012; Martinez-Rey et al., 2015; Kock et al., 2016).

N_2O distributions throughout the ocean are affected mainly by microbial production and consumption (Suntharalingam and Sarmiento, 2000), although N_2O produced in the deep ocean can be transported long distances, mixing between water masses before it is released to the atmosphere (e.g. Yamagishi et al., 2007; Nevison et al., 2003). In aerobic environments, N_2O can be generated by ammonia-oxidizing bacteria (AOB) or ammonia-oxiziding archaea (AOA) (Santoro et al., 2011; Löscher et al., 2012). AOB produce N_2O through hydroxylamine oxidation (referred to here as 'nitrification') and nitrite reduction (nitrifier-denitrification) mechanisms (Wrage et al., 2001; Stein and Yung, 2003). While the enzymology is still unknown, AOA appear to produce N_2O via a hybrid mechanism, combining oxidized and reduced substrates (Stieglmeier et al., 2014; Kozlowski et al., 2016; Trimmer et al., 2016; Frame et al., 2017). In

oxygen deficient zones (ODZs), with O_2 concentrations below 5 μM, N_2O production and consumption via denitrification are thought to co-occur, driving rapid turnover of dissolved N_2O (Farias et al., 2009; Babbin et al., 2015), though net consumption of N_2O in the ODZ core leads to some of the lowest concentrations of N_2O observed (Bourbonnais et al., 2017).

Despite the consumption of N_2O in the anoxic core of the ODZs, these regions are still regarded as net sources of N_2O, due to high production rates and large N_2O accumulations in the oxycline above the ODZ (Naqvi and Noronha, 1991; Farias et al., 2007; 2009; Arevalo-Martinez et al., 2015; Martinez-Rey et al., 2015). As multiple mechanisms may be operative under such conditions, understanding the controls on N_2O production and quantifying its release from these regions is difficult. N_2O can be produced via stop and go denitrification where fluctuations in O_2 concentration may promote NO_3^- and NO_2^- reduction to N_2O but inhibit N_2O reduction to N_2 (Codispoti and Christensen, 1985; Nicholls et al., 2007; Yamagishi et al., 2007; Naqvi et al. 2010). Under these conditions, N_2O yields from nitrifying bacteria may also be enhanced (Goreau et al., 1980; Lipschultz et al., 1990; Ji et al., 2015), although accumulation of NO_2^- may be a prerequisite (Frame and Casciotti, 2010). Deciphering the contributions of nitrification and denitrification in the oxycline of ODZs is essential to understanding greenhouse gas feedbacks associated with climate change and ocean acidification (Stramma et al., 2008; Beman et al., 2011; Freing et al., 2012; Wright et al., 2012).

N_2O stable isotope measurements are powerful tools with which to track its production and consumption mechanisms (Kim and Craig, 1993; Rahn and Wahlen, 2000; Yoshida and Toyoda, 2000; Farias et al., 2009; Yamagishi et al., 2007). The bulk isotopic signals include $\delta^{15}N^{bulk}$ and $\delta^{18}O_{N2O}$, where $\delta^{15}N^{bulk}$ (‰) = $(^{15}R_{N2O}/^{15}R_{std} - 1) \times 1000$ and $\delta^{18}O_{N2O}$ (‰) = $(^{18}R_{N2O}/^{18}R_{std} - 1) \times 1000$). The site-specific isotopic measurements include $\delta^{15}N^{\alpha}$ and $\delta^{15}N^{\beta}$,

where α is the central N atom and β is the outer N atom in the linear N_2O molecule (Toyoda and Yoshida, 1999). The bulk isotopic compositions are dependent on the substrates' isotopic compositions and the isotope effects of the process that produce and/or consume N_2O (Yoshida et al., 1984). An isotope effect (ε (‰) = ($^{L}k/^{H}k - 1$)* 1000) results from small differences in the rates at which molecules containing the light (^{L}k) and heavy (^{H}k) isotopes react, leading to predictable differences in the isotope ratios of the substrates and products of a reaction (Mariotti et al., 1981). The intramolecular distribution of N isotopes within N_2O complements the bulk isotope ratio analyses because the SP ($SP = \delta^{15}N^{\alpha} - \delta^{15}N^{\beta}$) is thought to be driven mainly by the production mechanism and not the isotopic composition of the substrate molecules (Toyoda and Yoshida, 1999; Schmidt et al., 2004; Sutka et al., 2003; 2006; Frame and Casciotti, 2010). This common assumption may break down, however, where N_2O is produced from two different substrates that may vary in $\delta^{15}N$ independently, such as through a hybrid mechanism (e.g., NH_4^+ and NO_2^-) (Stieglmeier et al., 2014, Kozlowski et al., 2016). In this case, variations in SP could be produced through a single process. Thus, N_2O isotopomeric measurements combined with isotopic measurements of potential substrates for N_2O should be used to identify the active N_2O production and consumption processes (Yamagishi et al., 2007; Westley et al., 2006; Farias et al., 2009; Bourbonnais et al., 2017).

The Eastern Tropical South Pacific (ETSP) is an eastern boundary coastal upwelling region (Fig. 1) that is known to be a major source of N_2O to the atmosphere (Bange et al., 1996; Nevison et al., 2004; Zamora et al., 2012; Arevalo-Martinez et al., 2015; Martinez-Rey et al., 2015). It has one of the shallowest (upper boundary 200 m), most intense ODZs (e.g. Farias et. al., 2007, 2009), a strong oxygen gradient, and intense N_2O accumulation. The primary objective of this study was to elucidate the physical (mixing, advection) and biological processes that

shape the distribution of N_2O in the ETSP. We analyzed natural abundance bulk isotopic compositions of N_2O ($\delta^{15}N^{bulk}$ and $\delta^{18}O_{N2O}$), as well as isotopomers of N_2O ($\delta^{15}N^{\alpha}$ and $\delta^{15}N^{\beta}$), and combined these with supporting measurements of NO_2^- and NO_3^- isotopic composition ($\delta^{15}N$ and $\delta^{18}O$), as well as hydrographic and nutrient data, to gain new insights into the sources and sinks of N_2O in and around the ETSP ODZ.

2. Materials and Methods

2.1 Field Sampling

Samples were collected aboard the R/V Nathaniel B. Palmer from June to July 2013 (cruise NBP1305) in the ETSP off Peru and northern Chile (Fig. 1). Salinity, potential temperature, and pressure data were recorded by the ship's conductivity, temperature, depth (CTD) sensors. Within the ODZ, [O_2] was below the detection limit of the SBE 43 O_2 sensor (~ 2 μM), and it is typically lower than the detection limit of the STOX sensor (< 10 nM) (Revsbech et al., 2009; Thamdrup et al., 2012; Tiano et al., 2014; Garcia-Robledo et al., 2016). Outside the ODZ, the [O_2] data from the SBE 43 were verified with Winkler titrations (Langdon et al., 2010) on 53 discrete samples that were collected during the cruise. The calibration slope was 0.956 (R^2 = 0.9998), and there was no evidence of sensor drift during the cruise (i.e., no significant trend in the residuals).

Concentrations of phosphate (PO_4^{3-}), nitrate (NO_3^-), and nitrite (NO_2^-) were measured at sea according to Gordon et al. (1993) including reagent preparation, calibration of lab ware, preparation of primary and secondary standards, and corrections for blanks and refractive index. Duplicate samples for NO_3^- isotopic analysis were collected from each station and depth, filtered (0.2 um pore size), and frozen on board, then shipped and stored frozen at Stanford University

125 until analysis (see Peters et al., 2018 for details). Duplicate samples for NO_2^- isotopic analysis
126 were also collected from depths containing measurable NO_2^- (> 0.1 μM). These samples were
127 reacted with sodium azide on board, in parallel with NO_2^- isotopic standards, and stored as N_2O
128 in sealed 20 mL headspace vials until analysis (see Peters et al., 2018 for details).
129 Duplicate samples were collected for dissolved N_2O concentration and stable isotopic
130 measurements from a subset of stations (4, 5, 17, 18, 20, Big Bag 1 (BB1) and Big Bag 2 (BB2))
131 (Fig. 1). Samples for dissolved N_2O analysis were subsampled into 160 mL Wheaton glass
132 serum vials from Niskin bottles by connecting Tygon tubing to the Niskin bottles. Each bottle
133 was filled to the top and overflowed twice without introduction of bubbles. After collection,
134 approximately 1 ml liquid was immediately removed to permit the addition of 100 μL of
135 saturated mercuric chloride ($HgCl_2$) solution and to allow for any expansion during storage. The
136 bottle was then sealed with a gray butyl septum (as above) and aluminum crimp seal (as above)
137 and stored at room temperature until analysis in the laboratory.
138
139 *2.2 Laboratory Analysis*
140 The amount (nmoles) of dissolved N_2O in each aqueous sample was determined via
141 calibration of the major ion peak area (mass-to-charge (m/z) ratio = 44) against m/z = 44 peak
142 areas of NO_3^- standards added in 2-20 nmole amounts and converted to N_2O via the denitrifier
143 method (McIlvin and Casciotti, 2010). In turn, the dissolved N_2O concentration (nmoles/L, or
144 nM) in the sample was determined using the volume of each sample extracted, determined by
145 weight (0.153 ± 0.003 L). The calibrated range of N_2O concentrations was thus 6.5–65 nM. In
146 addition, air-equilibrated seawater samples run with each batch of analyses yielded an average
147 concentration of 7.2 ± 1.1 nM, consistent with atmospheric equilibration at T = 18–23 °C.

148 N_2O isotopic analyses were made on a Finnigan Delta^{PLUS} XP isotope ratio mass
149 spectrometer at Stanford University. Samples were extracted, concentrated and delivered to the
150 IRMS under helium flow via the purge trap system described in McIlvin and Casciotti (2010).
151 Measurements of $\delta^{15}N^{bulk}$, $\delta^{18}O_{N2O}$, $\delta^{15}N^{\alpha}$, and $\delta^{15}N^{\beta}$ in N_2O were determined according to
152 McIlvin and Casciotti (2010) and calibrated according to Frame and Casciotti (2010) against
153 injections of calibrated N_2O reference gas with $\delta^{15}N^{\alpha}$ = 0.14‰ vs. air, $\delta^{15}N^{\beta}$ = -0.03‰ vs. air,
154 and $\delta^{18}O$ = 39.76‰ vs. VSMOW. Due to fragmentation and position scrambling of N_2O during
155 ionization in the source, the measured ratio of m/z 31 and 30 (from ^{15}N-$^{16}O^+$ and ^{14}N-$^{16}O^+$,
156 respectively) has contributions from both ^{14}N-^{15}N-^{16}O and ^{15}N-^{14}N-^{16}O (Toyoda and Yoshida
157 1999). However, the rate of fragmentation of ^{14}N-^{15}N-^{16}O and ^{15}N-^{14}N-^{16}O relative to ^{14}N-^{14}N-
158 ^{16}O can't be assumed equal, giving rise to fractionation factors that alter the measured 31/30
159 ratios relative to the abundances of ^{14}N-^{15}N-^{16}O, ^{15}N-^{14}N-^{16}O and ^{14}N-^{14}N-^{16}O (Westley et al.
160 2007). These fractionation factors have been determined for our instrument operating conditions
161 by dual inlet IRMS analysis of our calibrated N_2O reference gases (Frame and Casciotti, 2010)
162 and two additional N_2O reference gases (Mohn et al., 2014). Quality control checks for the
163 samples were made against daily analyses of air-equilibrated seawater samples, which yielded
164 $\delta^{15}N^{bulk}$, $\delta^{18}O_{N2O}$ and SP of 7.3 ± 0.5‰, 45.6 ± 0.7‰, 19.5 ± 1.5‰, respectively, for air-
165 equilibrated seawater (n = 70) in parallel with the seawater samples. Thus, our calibration yields
166 measurements of tropospheric N_2O similar to previous reports (Kim and Craig, 1993; Yoshida
167 and Toyoda, 2000; Sutka et al., 2004).
168 Nitrate isotope analyses were conducted at Stanford University using the denitrifier
169 method (Sigman et al., 2001; Casciotti et al., 2002), with modifications described in McIlvin and
170 Casciotti (2011), and referenced against 200 μM solutions of NO_3^- isotope reference materials

171 USGS32, USGS34, and USGS35. NO_2^- was removed using sulfamic acid (Granger and Sigman,
172 2009) prior to NO_3^- isotopic analysis for any sample containing measurable (> 0.1 μM) NO_2^-.
173 Nitrite isotope analyses were conducted at Stanford University on azide-preserved samples,
174 calibrated to azide-preserved NO_2^- isotope standards (N-23, N-7373, and N-10219; Casciotti et
175 al., 2007) prepared at sea. See Peters et al. (2018) for additional details.
176

177 ## 3. Results

178 *3.1 Spatial variation of oxygen, nitrite, and nitrous oxide in ETSP*

179 In the surface layer (0–60 m for most stations; 0–20 m for BB2) O_2 concentrations were
180 near equilibrium with the atmosphere (> 200 μM) (Fig. 2A). Through the oxycline
181 (approximately 60–120 m for most stations; 20–50 m for BB2), O_2 declined sharply reaching a
182 minimum (< 2 μM) at the top of the ODZ. Throughout the ODZ (120–400 m for most stations;
183 50–400 m for Big Bag 2) O_2 concentrations remained < 2 μM. Below the ODZ (> 400 m) O_2
184 concentrations increased with depth background concentrations near 100 μM.

185 Nitrite (NO_2^-) concentrations were < 1 μM in the surface layer and peaked in
186 concentration (4–7.5 μM) with a secondary NO_2^- maximum (SNM) in the ODZ core at most
187 stations (4, 5, 17, 18, BB1 and BB2) (Fig. 2B). No measurable SNM peak was identified at
188 station 20. Below the ODZ (> 400 m) NO_2^- concentrations were undetectable (< 0.1 μM) at all
189 stations. The presence of a SNM at most stations suggests that the ODZ becomes functionally
190 anoxic, reaching O_2 concentrations well below the detection limit of the SBE-43 sensor, most
191 likely less than 50 nmol/kg (Thamdrup et al., 2012).

192 Surface water N_2O concentrations ranged between 7–10 nM (Fig. 2C). Calculated N_2O
193 saturations with respect to atmosphere N_2O (Weiss and Price 1980) indicate that all station

surface waters were close to or slightly above atmospheric equilibrium (95−120% saturation). Increases in N_2O concentrations (N_2O saturation 200−500 % with respect to atmosphere N_2O) were observed in the oxycline, reaching a maximum of 48−68 nM at the top of the ODZ (100−120 m). Within the ODZ, the N_2O concentrations fell to minima of 6−9 nM (N_2O saturation 60−90% with respect to atmospheric N_2O) at ~300 m. The exception was Station 20 where N_2O concentrations dropped only to 20 nM and saturation remained above 200% throughout the oxygen minimum. At the base of the ODZ (400 m), a secondary N_2O concentration maximum (60 nM) was observed at all stations (N_2O saturation up to 500%). Below this peak, N_2O concentrations decreased with depth down to 20−30 nM N_2O (saturation down to approximately 200%).

Based on the characteristics of the O_2, NO_2 and N_2O concentration profiles, data from all stations were divided into four layers by density: surface (σ_θ = 25.3−25.6 kg/m^3), oxycline (σ_θ = 25.6−26.2 kg/m^3), ODZ (σ_θ = 26.2−26.8 kg/m^3) and deep (below σ_θ = 26.8 kg/m^3). The surface layer contained generally uniform distributions of O_2 and N_2O concentrations. The oxycline layer contained decreasing O_2 and increasing N_2O concentrations, but no NO_2^-. The ODZ contained the lowest O_2, decreasing and low N_2O concentrations, as well as the accumulated NO_2^-. The deep layer included all samples falling below the ODZ layer. Further divisions were made within the ODZ between the upper (σ_θ = 26.2−26.4 kg/m^3, decreasing N_2O), middle (σ_θ = 26.4−26.6 kg/m^3, N_2O minimum) and lower (σ_θ = 26.6−26.8 kg/m^3, N_2O increasing to the lower maximum) portions, and will be referred to throughout the discussion.

3.2 Isotopic composition of N_2O

The bulk $\delta^{15}N$ of N_2O ($\delta^{15}N^{bulk}$) in surface waters (< 60 m) was similar to that of

atmospheric N_2O (Kim and Craig, 1993; Yoshida and Toyoda, 2000; Sutka et al., 2004) (Fig. 3). $\delta^{15}N^{bulk}$ values generally decreased from the surface to a subsurface minimum near 6‰ (Fig. 3A) at the peak in N_2O concentration (Fig. 2C). $\delta^{15}N^{bulk}$ then increased to greater than 20‰ in the ODZ before falling to ~6‰ at the base of the ODZ (400 m). At station BB2 the peak in $\delta^{15}N^{bulk}$ (> 20‰) was observed at a shallower depth (100 m), coincident with a shallower ODZ and N_2O concentration minimum, and a subsurface $\delta^{15}N^{bulk}$ minimum was not observed. Below 400 m, $\delta^{15}N^{bulk}$ gradually increased with depth to values of approximately 10‰ at all stations.

$\delta^{18}O_{N2O}$ values were lowest at the surface (~50‰ VSMOW) and did not show a minimum in the oxycline. $\delta^{18}O_{N2O}$ increased steadily from the base of the oxycline, and remained elevated throughout the ODZ (Fig. 3B) coinciding with low N_2O concentrations. At the ODZ core, $\delta^{18}O_{N2O}$ values ranged from 68−100‰, with most stations displaying a peak in enrichment between 200−400 m, except station BB2, which displayed a peak in $\delta^{18}O_{N2O}$ at a shallower depth (100 m) than other stations, as well as a second peak in the lower ODZ. Station 20 showed a smaller $\delta^{18}O_{N2O}$ enrichment, consistent with the smaller decrease in N_2O concentration. Below the ODZ, $\delta^{18}O_{N2O}$ values decreased with depth, approaching 50−60‰ in deeper waters at all stations.

Site preference (SP) distributions had some features that followed $\delta^{15}N^{bulk}$ and others that followed $\delta^{18}O_{N2O}$ (Fig. 3C). In the surface waters, SP values were variable (10−20‰) compared to those expected for atmospheric equilibrium (~18.7‰, Westley et al., 2007). In the oxycline (40 m for BB2, 60−80 m for other stations), SP displayed minimum values (< 10 ‰) coincident with the primary N_2O peak and local minimum in $\delta^{15}N^{bulk}$. Like $\delta^{18}O_{N2O}$, SP increased below the oxycline displaying a broad maximum across the ODZ (200−400 m). In contrast, $\delta^{15}N^{bulk}$ reached a sharp peak in the upper ODZ and showed a decreasing trend through the lower ODZ.

240 Like $\delta^{18}O_{N2O}$, SP also showed a double peak structure at station BB2. Below 500 m, SP values
241 decreased to 20–25‰ at all stations.
242 $\delta^{15}N^{\alpha}$ values (Fig. 3D) also showed some features that tracked $\delta^{15}N^{bulk}$ and others that
243 tracked $\delta^{18}O_{N2O}$. $\delta^{15}N^{\alpha}$ ranged between 15‰ and 18‰ in surface waters at each station. At
244 stations 5, 18 and BB1 $\delta^{15}N^{\alpha}$ values decreased to minima near 11‰ in the oxycline before
245 increasing to 30–40‰ in the ODZ. $\delta^{15}N^{\alpha}$ values remained high throughout the ODZ, then
246 decreased to a local minimum at 400 m before gradually increasing to uniform values near 20‰
247 in deep water.
248 $\delta^{15}N^{\beta}$ showed the most distinctive pattern. It ranged between -1‰ and -3‰ in surface
249 waters, and increased to 2–4‰ in the oxycline and upper ODZ (Fig. 3E). This was followed by a
250 decrease in $\delta^{15}N^{\beta}$ through the core and lower ODZ (-10 to -20‰), before returning to -1 to -3‰
251 in deep waters. At station BB2, $\delta^{15}N^{\beta}$ values were more dynamic with the upper ODZ displaying
252 a minimum in $\delta^{15}N^{\beta}$ near -8‰, followed by a return to positive values (2‰) in the ODZ core,
253 before decreasing to -18‰ in the lower ODZ (Fig. 3E). Positive $\delta^{15}N^{\beta}$ values ranging between 3
254 and 5‰ were observed in the upper ODZ for stations 4 and 20. Interestingly, $\delta^{15}N^{\beta}$ values
255 remained relatively constant in the upper ODZ while N_2O concentration decreased and $\delta^{15}N^{\alpha}$,
256 SP, and $\delta^{18}O_{N2O}$ increased dramatically. In the middle of the ODZ, $\delta^{15}N^{\beta}$ and $\delta^{15}N^{\alpha}$ decreased,
257 while SP remained the same, or continued to increase, and $\delta^{18}O_{N2O}$ decreased slightly. In the
258 lower ODZ, $\delta^{15}N^{\beta}$ increased while $\delta^{15}N^{\alpha}$, SP, and $\delta^{18}O_{N2O}$ decreased.
259

260 ## 4. Discussion

261 *4.1 Determining the isotopic and isotopomer ratio of produced N_2O*

To elucidate the processes responsible for the production of N_2O in the surface, oxycline, and deep samples, a two end-member mixing model was applied (Keeling, 1961; Pataki et al., 2003; Yamagishi et al., 2007, Fujii et al., 2013). The so-called Keeling plot method assumes a uniform background pool of N_2O ($N_2O_{background}$) to which new N_2O is added ($N_2O_{produced}$), tracking both the concentration (equation 1) and the isotopic composition (equation 2) of N_2O. One can determine the isotopic composition of the N_2O produced within a given water mass from the intercepts of the linear relationships between the inverse of the observed N_2O concentration ($1/[N_2O_{observed}]$) and the $\delta^{15}N^{bulk}$, $\delta^{18}O_{N2O}$, or SP observations (equation 3).

$$[N_2O_{observed}] = [N_2O_{background}] + [N_2O_{produced}] \quad (1)$$

$$\delta_{observed} * [N_2O_{observed}] = \delta_{background} * [N_2O_{background}] + \delta_{produced} * [N_2O_{produced}] \quad (2)$$

$$\delta_{observed} = 1/[N_2O]_{observed}] * (\delta_{background} - \delta_{produced}) * [N_2O_{background}] + \delta_{produced} \quad (3)$$

Where $[N_2O]$ represents nitrous oxide concentration and δ is the isotopic composition (either $\delta^{15}N^{bulk}$, $\delta^{18}O_{N2O}$, or SP), and the subscripts indicate whether the observe signal is from 'background' or subsequently 'produced' N_2O. Uncertainty analysis is provided by the 95% confidence interval of the linear fit parameters (Fig. 4; Table 1). Assumptions about a uniform background that go into the Keeling plot method could be tested by comparing the N_2O concentration or isotopic compositions of the background N_2O to those calculated from the slope of equation (3). However, the 95% confidence interval of the slopes in most cases were quite large and did not lend themselves to further calculations about the background conditions.

For the Keeling plot analysis, the surface, oxycline and deep layers were treated as isolated waters that have negligible mixing between them, and data from all stations (except

285 coastal BB2, which showed a different N_2O depth profile) were combined within these layers.
286 Keeling plot analysis was unsuitable for the ODZ layer, due to N_2O consumption being a
287 dominant process in this zone (Yamagishi et al., 2007; Farias et al., 2009; Babbin et al., 2015;
288 Bourbonnais et al., 2017). We will return to analysis of the ODZ data later in the discussion.
289 $\delta^{15}N^{bulk}$ of produced N_2O is dependent on the $\delta^{15}N$ of the substrates, as well as the
290 fractionation factors associated with the formation pathways (Yoshida et al., 1984; Stein and
291 Yung, 2003; Sutka et al., 2006; Fujii et al., 2013; Frame et al., 2014; Bourbonnais et al., 2017).
292 The $\delta^{15}N^{bulk}$ values of $N_2O_{produced}$ here were similar between the surface (6.1 ± 1.4‰), oxycline
293 (7.5 ± 2.2‰), and deep (6.6 ± 0.6‰) layers (Fig. 4A; Table 1). The produced $\delta^{15}N^{bulk}$ values
294 were also similar to those of sinking particulate organic matter (POM) in the ETSP (4–11‰;
295 Berelson et al., 2015), with the NH_4^+ released from it likely 2–3‰ depleted in ^{15}N (Altabet,
296 1988; Montoya et al., 2002). Production of N_2O during nitrification yields $\delta^{15}N^{bulk}$ that is similar
297 to or lower than $\delta^{15}N$ of the NH_4^+ substrate, depending on the net isotope effect expressed during
298 this multi-step process (Ostrom and Ostrom, 2012). Therefore, if N_2O here derives from
299 nitrification, it would require a low net isotope effect, such as that dominated by diffusion
300 (Ostrom and Ostrom, 2012). Denitrification or nitrifier-denitrification may also be responsible
301 for the produced N_2O (Farias et al., 2009; Ji et al., 2015; Bourbonnais et al., 2017). We would
302 expect the $\delta^{15}N^{bulk}$ of N_2O produced during denitrification or nitrifier-denitrification to be lower
303 than the substrates (NO_2^- and NO_3^-), though the net isotope effects between NO_2^- or NO_3^- and
304 N_2O are highly variable, depending on the relative rates of the intermediate steps (Ostrom and
305 Ostrom, 2012). $\delta^{15}N^{bulk}$ was generally lower than co-occurring NO_3^- (5–32‰; Peters et al.,
306 2018), and higher than co-occurring NO_2^-, but given the wide uncertainty in the source values,
307 and the narrow range of $\delta^{15}N^{bulk}$ values observed in our dataset (Fig. 3A; Fig. 4A), it is difficult

to identify the source(s) of N_2O based on $\delta^{15}N^{bulk}$ alone.

The $\delta^{18}O$ of $N_2O_{produced}$ was slightly lower in the oxycline (50.7 ± 3.6‰) than in the surface (53.0 ± 3.0‰) and deep layers (54.3 ± 0.6‰) (Fig. 4B; Table 1). $\delta^{18}O_{N2O}$ reflects the $\delta^{18}O$ values of N_2O sources: O_2 and H_2O during nitrification, and NO_2^- or NO_3^- during denitrification, along with the isotopic fractionation during N_2O production and O isototope equilibration (Ostrom et al., 2000; Wrage et al., 2001; Frame and Casciotti, 2010; Snider et al., 2012; Casciotti and Buchwald, 2012). $\delta^{18}O_{N2O}$ values were indeed elevated relative to potential substrates (O_2, H_2O, NO_2^-, NO_3^-), which may be expected due to preferential loss of ^{16}O during N-O bond cleavage steps between NO_3^- and N_2O during denitrification (Casciotti et al., 2002; Casciotti and McIlvin, 2007; Toyoda et al., 2005). Expected $\delta^{18}O_{N2O}$ values from nitrification and nitrifier denitrification are typically lower, ranging from 13−35‰ (Snider et al., 2012). A source with lower $\delta^{18}O$, such as that in the oxycline, may be attributable to nitrifier-denitrification or denitrification with H_2O contributing to the substrate NO_2^- (Ostrom et al., 2000). A stronger contribution from denitrification or nitrifier-denitrification would also be consistent with some of the lowest $\delta^{15}N^{bulk}$ values observed in the oxycline, as N_2O with low $\delta^{15}N^{bulk}$ is commonly observed during nitrifier-denitrification (Yoshida, 1988; Webster and Hopkins, 1996; Sutka et al., 2004; Frame and Casciotti, 2010).

N_2O SP is thought to mainly reflect the production mechanisms, independent of the precursors' isotopic composition (Yoshida and Toyoda, 2000; Schmidt et al., 2004; Sutka et al., 2004). Thus, it has been a powerful tool for differentiating N_2O contributions from oxidative (nitrification) and reductive (denitrification and nitrifier-denitrification) pathways (Sukta et al., 2006; Ostrom et al., 2007). N_2O produced during nitrification has SP between 30‰ and 38‰ (Sukta et al., 2003, 2004; Frame and Casciotti, 2010), while production via denitrification and

nitrifier-denitrification results in SP of -10‰ to 25‰ (Sukta et al., 2003, 2004; Toyoda et al., 2005; Frame and Casciotti, 2010). N_2O produced by ammonia-oxidizing archaea (~30‰) is similar to that from nitrification by ammonia-oxidizing bacteria (Santoro et al., 2011; Löscher et al., 2012). The Keeling plot analysis suggests that the SP of $N_2O_{produced}$ increased from the surface (5.4 ± 4.4‰) and the oxycline (9.3 ± 2.4‰) into the deep (20.2 ± 0.5‰) layers (Fig. 4C; Table 1). This increase in SP would thus indicate a greater contribution of nitrification to N_2O production in the deep layer compared with the surface and oxycline, which both show a stronger influence of denitrification or nitrifier-denitrification. This is consistent with the above discussion of $\delta^{15}N^{bulk}$ and $\delta^{18}O$ in the oxycline supporting denitrification or nitrifier-denitrification as an important source of N_2O. However, if hybrid N_2O from archaea is an important source of N_2O in the oxycline (Stieglmeier et al., 2014; Trimmer et al., 2016; Frame et al., 2017), then SP may be set by the relative $\delta^{15}N$ values of the substrates for the α and β positions, rather than being a proxy for a particular source.

In summary, the excess N_2O (100−120%) in the surface layer may be due to either in situ production or upward mixing from the N_2O peak in the oxycline. The low SP value of the source N_2O suggests that denitrification or nitrifier denitrification are likely contributing to the N_2O excess in this layer. N* (N* = $[NO_3^-]$ + $[NO_2^-]$ – 16*$[PO_4^-]$ + 2.9 μmol kg^{-1}), the fixed N (NO_3^- and NO_2^-) excess or deficit relative to the mean ocean relationship with PO_4^{3-} (e.g. Gruber and Sarmiento, 1997, Deutsch et al., 2001), was negative (-6.0 to -9.6 μmol kg^{-1}) at these sites. This implies that there has been some interaction between the surface waters and the lower oxygen region below that supports denitrification. In the oxycline, significant N_2O saturation (200−500%) with respect to the atmosphere and peak $[N_2O]$ values of in excess of 50 nM, imply net N_2O production within the oxycline. The similarity of isotopic compositions in the oxycline

and surface layer N_2O source values suggests again that denitrification and/or nitrifier denitrification are likely contributing to the N_2O excess in this layer, consistent with earlier isotopic measurements (Bourbonnais et al., 2017) and isotope tracer experiments during this cruise (Ji et al., 2015). Further, the similarity in isotopic composition between the surface and oxycline support the idea of exchange between the two, driving the surface layer N_2O supersaturation and high surface fluxes of N_2O in the ETSP (Averalo-Martinez et al., 2015). The slightly higher SP source (9‰) in the oxycline may be indicative of co-occurring production and consumption by denitrification, with the increases in SP and $\delta^{15}N^{bulk}$ reflecting the effect of consumption. In the deep layer, N_2O concentrations ranged between 19.7−59.0 nM with saturation levels ranging from 244−590%. The higher SP values reflect a likely increased contribution of nitrification, potentially by archaea, to background N_2O production below the ODZ.

4.2 Elucidation of N_2O cycling within the ODZ

The elevated $\delta^{15}N^{bulk}$, $\delta^{18}O_{N2O}$ and SP values observed in the ODZ, combined with lower N_2O concentrations, are interpreted to reflect N_2O consumption via denitrification (Yamagishi et al., 2007; Farias et al., 2009). Linear relationships between $\delta^{18}O_{N2O}$ and $\delta^{15}N^{\alpha}$, as well as $\delta^{18}O_{N2O}$ vs. SP are expected for N_2O consumption via denitrification due to the breakage of the O-N^{α} bond during N_2O reduction (Ostrom et al., 2007). This leads to concomitant increases in $\delta^{15}N^{\alpha}$ and $\delta^{18}O_{N2O}$. As N_2O reduction does not involve breakage of bonds to N^{β}, N_2O reduction is expected to have much less effect on $\delta^{15}N^{\beta}$ (Ostrom et al., 2007). A linear relationship was indeed observed between $\delta^{18}O_{N2O}$ and $\delta^{15}N^{\alpha}$, with a slope of 1.74 ± 0.14, which is similar to the 1.7−1.9 slope expected for N_2O consumption via denitrification (Ostrom et al., 2007; Jinuntuya-

377 Nortman et al., 2008) (Fig. 5A). However, the observed relationship between $\delta^{18}O_{N2O}$ and SP
378 (Fig. 5B) was only 1.15 ± 0.09, which was considerably lower than slopes previously observed
379 for denitrification in culture (2.2; Ostrom et al., 2007) and soil mesocosms (1.3–3.3; Lewicka-
380 Szczebak et al., 2017). In our study, within the ODZ at the N_2O concentration minimum, $\delta^{18}O_{N2O}$
381 values were lower than expected for the observed SP values.

382 The lower than expected $\delta^{18}O_{N2O}$ (or higher than expected SP) in the ODZ could be due
383 to a number of factors. First, mixing between regional water masses that possess different N_2O
384 production and consumption histories (Carrasco et al., 2017) may lead to higher SP enrichment
385 relative to the corresponding $\delta^{18}O_{N2O}$. This could explain the observed $\delta^{18}O$ vs. SP pattern if one
386 of the water masses dominating the ODZ (see below) had a higher starting SP value for its
387 $\delta^{18}O_{N2O}$ (Fig. 5B, 'ESSW source water'). Second, the ^{18}O isotope effect for N_2O reduction ($\varepsilon^{18}O$)
388 could decrease relative to the isotope effect for SP (εSP) at lower N_2O concentrations, causing a
389 slower $\delta^{18}O_{N2O}$ increase relative to SP at higher extents of N_2O consumption. Finally, production
390 of N_2O within the ODZ could result in the lowering of $\delta^{18}O_{N2O}$ relative to SP or increasing SP
391 relative to $\delta^{18}O_{N2O}$. For example, a process depleting $\delta^{15}N^{\beta}$ could increase SP independently of
392 $\delta^{15}N^{\alpha}$ and $\delta^{18}O_{N2O}$. Where $\delta^{15}N^{\beta}$ remains constant, changes in SP rely on changes in $\delta^{15}N^{\alpha}$ (and
393 $\delta^{18}O_{N2O}$ since they are linked; Fig. 5A). However, where $\delta^{15}N^{\beta}$ decreases, SP can increase
394 regardless of changes in $\delta^{15}N^{\alpha}$ (and $\delta^{18}O_{N2O}$). Each of these potential explanations is discussed
395 below.
396
397 *4.2.1 Potential for water mass mixing in the ODZ*

398 In order to understand the potential role of water mass mixing on N_2O isotope
399 distributions in the ODZ, we drew on a recent water mass analysis for this cruise (Peters et al.,

2018). Optimum multi-parameter analysis (OMPA) is a tool that has been developed for determining the contributions of source waters to a given location (e.g. Karstensen and Tomczak, 1998; Mackas et al., 1987; Tomczak and Large, 1989). OMPA involves the construction of a set of linear mixing equations from conserved water mass properties, and solving for the fractions of the water masses in question. Peters et al. (2018) quantified the proportions of two water mass end members in the ETSP ODZ: Equatorial Subsurface Waters (ESSW) and Eastern South Pacific Intermediate Waters (ESPIW) following water mass definitions from previous work (De Pol-Holz et al., 2007; Silva et al., 2009; Llanillo et al., 2013). ESSW waters move south from the equator in the Peru-Chile Undercurrent, while ESPIW is transported north towards the equator in the Humboldt Current, with the two waters converging in the ODZ off the Peruvian coast (Silva et al., 2009; Czeschel et al., 2011; Llanillo et al., 2013; Grasse et al., 2013). These water masses generally ride above the Antarctic Intermediate Waters (AAIW), which contains the deep N_2O concentration maximum (Carrasco et al., 2017).

Relationships of ESSW (as a percentage of the water sample) with salinity, and dissolved O_2 and N_2O concentrations were varied (Fig. S1). Salinity displayed a mostly linear relationship with ESSW water mass percentage, as expected for a conservative parameter. In comparison, O_2 and N_2O concentrations relationships with ESSW water mass percentage were distinctly non-linear. O_2 concentrations remained at the limit of detection between 70–95% ESSW, and increased below 70% ESSW. N_2O concentrations were generally anti-correlated with % ESSW, but showed a peak of N_2O concentration within the upper oxycline at 70% ESSW. This suggests that while ESSW water mass percentage appears to play some role in the geochemical signature of the ODZ, biogeochemical processes in and around the ODZ also contribute to the observed distributions of chemical species. Further, for mixing to explain the deviation of $\delta^{18}O_{N2O}$ and SP

423 from the expected relationship driven by N_2O reduction, the N_2O in ESSW source water would
424 need to have a high SP (50‰) for its $\delta^{18}O_{N2O}$ value (~50‰) (Fig. 5B). While much of the deep
425 ocean has a $\delta^{18}O_{N2O}$ near 50‰, SP values of this magnitude are only observed in ODZ's where
426 $\delta^{18}O_{N2O}$ values are much higher (Yamagishi et al., 2007; Farias et al., 2009; Bourbonnais et al.,
427 2017). The combination of $\delta^{18}O_{N2O}$ and SP values required to explain the pattern through mixing
428 alone has not been observed in the Pacific Ocean (Yamagishi et al., 2005; 2007, Toyoda et al.,
429 2002; Fujii et al., 2013, Popp et al., 2002; Farias et al., 2009).
430
431 *4.2.2. Variable isotope effects (ε) during N_2O consumption between low and high N_2O*
432 *concentrations*
433 As noted above, a deviation of $\delta^{18}O_{N2O}$ from the expected relationship with SP during
434 denitrification (Ostrom et al., 2007; Jinuntuya-Nortman et al., 2008) was identified for samples
435 with the lowest N_2O concentrations (< 30 nM; Fig. 5B), in the middle ODZ. The samples with
436 elevated SP and $\delta^{18}O_{N2O}$ values also exhibited low O_2 (< 2 μM) and high NO_2^- (> 2.0 μM)
437 concentrations. We investigated whether changes in the isotope effects for SP (εSP) and $\delta^{18}O_{N2O}$
438 ($\varepsilon^{18}O$) during N_2O consumption might have changed between the upper, middle, and lower ODZ
439 layers, corresponding to these different chemical environments.
440 The isotope effects were determined by performing linear regressions of SP or $\delta^{18}O_{N2O}$
441 vs. $-\ln[N_2O]$ assuming a closed-system Rayleigh model for each layer (eq. 4).
442 $$\delta_{N2O} = \delta_{N2O,0} - \varepsilon * \ln([N_2O]/[N_2O]_0) \quad (4)$$
443 Where δ_{N2O} corresponds to the $\delta^{18}O_{N2O}$ or SP for samples measured within a given isopycnal
444 layer, and $[N_2O]$ is the measured N_2O concentration (in nmol/L). $\delta_{N2O,0}$ and $[N_2O]_0$ are
445 hypothetical background concentration and isotopic values, prior to the onset of N_2O

446 consumption. This model assumes that N_2O consumption occurs in isolation of N_2O production
447 in the ODZ, and is a test of the hypothesis that the observed patterns may be due to N_2O
448 consumption alone. The potential for N_2O production in the ODZ will be discussed in more
449 detail below.

450 While $\varepsilon^{18}O$ values decreased consistently from upper to middle and lower ODZ layers
451 (25.6 ± 6.5‰, 19.6 ± 4.5 ‰, and 14.5 ± 3.4‰, respectively; Fig. 6A; Table 2), εSP values
452 increased slightly between the upper (17.5 ± 5.5 ‰) and middle ODZ (21.7 ± 3.1 ‰) layers
453 before decreasing markedly in the lower ODZ (11.6 ± 2.9 ‰; Fig. 6B; Table 2). These shifts in
454 $\varepsilon^{18}O$ and εSP between ODZ layers lead to similar ratios of $\varepsilon^{18}O$ to εSP in the upper (1.46 ± 0.56)
455 and lower ODZ (1.25 ± 0.45), which are both lower than the expected slope of 2.2 for N_2O
456 reduction during denitrification in culture (Ostrom et al., 2007) and near the lower end of the
457 range of values found in soil mesocosms (1.3–3.3; Lewicka-Szczebak et al., 2017). Furthermore,
458 the relative increase in εSP in the middle ODZ leads to a ratio of $\varepsilon^{18}O$ to εSP that is still lower
459 (0.90 ± 0.36; Table 2). When considering the transition to lower N_2O, lower O_2, and higher NO_2^-
460 concentrations within the middle ODZ, the apparent isotope effect for SP increases relative to
461 that for $\delta^{18}O$, further shifting the isotopic relationships away from that expected for N_2O
462 reduction by denitrifying bacteria (Ostrom et al., 2007). To better understand this shift in the SP
463 fractionation we now discuss the contributions of $\delta^{15}N^{\alpha}$ and $\delta^{15}N^{\beta}$ to the SP variations in the
464 ODZ.
465
466 *4.2.3. Dependence of SP on $\delta^{15}N^{\beta}$*
467 Up to now the increase in SP has been assumed to be driven by the same process that
468 causes an increase in $\delta^{18}O_{N2O}$, namely N_2O consumption. This would occur through an increase

469 in $\delta^{15}N^{\alpha}$ that parallels $\delta^{18}O_{N2O}$ during N-O bond breaking (Ostrom et al., 2007). Given that $\delta^{15}N^{\alpha}$
470 and $\delta^{18}O_{N2O}$ increase in concert with a slope roughly expected for denitrification (1.7; Fig. 5A),
471 while SP does not (Fig. 5B), we return to the idea that processes other than N_2O consumption
472 could be contributing to SP variations in the ODZ. Inspection of the $\delta^{15}N^{\alpha}$ and $\delta^{15}N^{\beta}$ profiles for
473 individual stations yields additional insight into the controlling factors (Fig. 7). It can be seen
474 that in the lower oxycline and upper part of the ODZ (σ_θ = 26.2–26.4 kg m^{-3}), SP, $\delta^{15}N^{\alpha}$, and
475 $\delta^{18}O_{N2O}$ increase simultaneously where N_2O concentrations are generally decreasing. In contrast,
476 $\delta^{15}N^{\beta}$ remains relatively constant and close to zero in this layer. Here, in the upper ODZ, the
477 increase in SP is driven by an increase in $\delta^{15}N^{\alpha}$, in parallel with $\delta^{18}O_{N2O}$, consistent with N_2O
478 consumption by denitrification (Fig. 5A). In the ODZ core (σ_θ = 26.4–26.6 kg m^{-3}), where N_2O
479 concentrations remain at relatively constant low values, SP and $\delta^{15}N^{\alpha}$ deviate from each other,
480 with SP remaining constant or continuing to increase, while $\delta^{15}N^{\alpha}$ begins to decrease. Here
481 $\delta^{15}N^{\beta}$ also becomes depleted in ^{15}N (-10‰), largely balancing the decrease in $\delta^{15}N^{\alpha}$, and
482 resulting in SP remaining unchanged in some cases and increasing slightly in others. These
483 patterns also reflect the sharp decrease in $\delta^{15}N^{bulk}$ while SP shows a broader maximum in the
484 ODZ. In this region, $\delta^{18}O_{N2O}$ also becomes slightly depleted relative to the peak value,
485 decoupling SP from $\delta^{18}O_{N2O}$ in this zone. In the lower ODZ, (σ_θ = 26.6–26.8 kg m^{-3}), $\delta^{15}N^{\alpha}$
486 continued to decrease while $\delta^{15}N^{\beta}$ increased to background values, leading to lower SP values as
487 $\delta^{15}N^{\alpha}$ and $\delta^{15}N^{\beta}$ approached each other. $\delta^{18}O_{N2O}$ also decreased to background values in this
488 zone.

489 The patterns in $\delta^{15}N^{\alpha}$, $\delta^{15}N^{\beta}$, and $\delta^{18}O_{N2O}$ thus provide insight into the causes of the
490 deviation in the $\delta^{18}O_{N2O}$ vs. SP relationship from that expected from N_2O reduction alone. Only

491 in the upper ODZ do the SP and $\delta^{18}O_{N2O}$ values follow those expected for pure N_2O
492 consumption (increasing $\delta^{15}N^{\alpha}$ and $\delta^{18}O_{N2O}$, unchanged $\delta^{15}N^{\beta}$) (Fig. 7). In the lower ODZ, $\delta^{15}N^{\alpha}$
493 and $\delta^{18}O_{N2O}$ both decrease, but $\delta^{15}N^{\beta}$ shows an opposite trend. In the middle ODZ, changes in
494 $\delta^{15}N^{\alpha}$ and $\delta^{18}O_{N2O}$ track each other, but they became decoupled from changes in SP due to
495 decreasing $\delta^{15}N^{\beta}$ values, which maintain the high SP. This is particularly clear at station BB1,
496 where SP remains elevated in the middle ODZ while $\delta^{15}N^{\beta}$, $\delta^{15}N^{\alpha}$, and $\delta^{18}O_{N2O}$ all decrease (Fig.
497 7A).

498 Similar trends of decreasing $\delta^{15}N^{\beta}$ coincident with elevated $\delta^{18}O_{N2O}$ and SP values have
499 been observed previously in the ETSP ODZ (Farias et al., 2009; Bourbonnais et al., 2017), as
500 well as anoxic zones in the Black Sea (Westley et al., 2006), the ETNP (Yamagishi et al., 2005;
501 2007), and Gulf of California (Yamagishi et al., 2007), where the signals have been interpreted
502 as reflecting concurrent N_2O production and consumption in the ODZ regions, consistent with
503 short-term rate measurements (Farias et al., 2009; Babbin et al., 2015). This is a logical
504 explanation given that the amount of N_2 produced exceeds the amount of N_2O that has
505 disappeared, indicating a need for additional production of N_2. If that derives from anammox,
506 this would not be associated with N_2O production. However, denitrification of NO_3^- or NO_2^-
507 would produce N_2O as an intermediate.
508
509 *4.2.4. Interpretation from measurements of nitrate and nitrite isotopes*
510 Multiple lines of evidence point to concurrent N_2O production and consumption by
511 denitrification to explain the distribution of N_2O and its isotopic composition in ODZs (Farias et
512 al., 2009; Babbin et al., 2015; Bourbonnais et al., 2017). Instantaneous rate measurements
513 indicate a high potential for N_2O production (Farias et al., 2009; Ji et al., 2015) and consumption

514 (Farias et al., 2009; Babbin et al., 2015) in ODZs and suggest rapid turnover of N_2O. With high
515 turnover rates, the ODZ N_2O pool should approach isotopic steady state, where concentrations
516 and isotopic ratios of N_2O remain constant due to tight cycling. This being the case, the N_2O
517 isotopic composition should reflect a balance of the isotopic signatures of N_2O sources (from
518 NO_3^- or NO_2^-) and sinks via denitrification. On the other hand, if N_2O consumption rates exceed
519 N_2O production, one would expect to observe enhanced expression of the kinetic isotope effects
520 for N_2O consumption. Here we test potential sources and cycling of N_2O within the ETSP ODZ
521 using parallel measurements of $\delta^{15}N$ and $\delta^{18}O$ in NO_3^- and NO_2^- (Peters et al., 2018).

522 Measurements of $\delta^{15}N_{NO2}$ in the ODZ at each station showed values between -10‰ and -
523 30‰ (Fig. 8A, gray boxes), while measured $\delta^{15}N_{NO3}$ was between 10–30‰ (Fig. 8A, red boxes).
524 $\delta^{15}N^{\alpha}$ ranged from 20–40‰ (Fig. 8A, blue boxes). If N_2O was in steady state with respect to
525 production from NO_2^-, and reduction to N_2, its isotopic composition should reflect the isotopic
526 composition of NO_2^-, as modified by isotopic fractionation between NO_2^- and N_2O, as well as
527 during N_2O consumption (Supplemental Information). For this analysis, the kinetic isotope effect
528 for NO_2^- reduction to $\delta^{15}N^{\alpha}$ was assumed to be 0‰ and the isotope effect for N_2O reduction was
529 assumed to be 9.1‰ for N^{α} (Ostrom et al., 2007). With this set of assumptions, the $\delta^{15}N^{\alpha}$ of N_2O
530 produced from NO_2^- at steady state (Fig. 8A, gray lines) is much lower than measured $\delta^{15}N^{\alpha}$
531 (Fig. 8A, blue boxes). Moreover, laboratory experiments suggest that the N isotope effect for
532 NO_2^- reduction is 8–20‰ (Bryan et al., 1983; Martin and Casciotti, 2016). If these isotope
533 effects are used instead of 0‰ fractionation during N_2O production from NO_2^-, the predicted
534 steady state $\delta^{15}N^{\alpha}$ would be even lower than the modeled $\delta^{15}N^{\alpha}$ values shown.

535 N_2O produced from NO_3^- was estimated to have a steady state $\delta^{15}N^{\alpha}$ of 20–30‰ (Fig 8A,
536 red lines) when the expressed N isotope effect for NO_3^- reduction to N_2O is assumed to be 0‰

and the isotope effect for $\delta^{15}N^{\alpha}$ during N_2O consumption is assumed to be -9.1‰ (Ostrom et al., 2007). This source of N_2O is much higher than that produced from NO_2^-, and it is in line with measured $\delta^{15}N^{\alpha}$ (Fig. 8A, blue boxes). Applying accepted kinetic isotope effects of 15–25‰ for NO_3^- reduction would cause modeled $\delta^{15}N^{\alpha}$ to decrease relative to measured $\delta^{15}N^{\alpha}$ values. Thus, the $\delta^{15}N^{\alpha}$ data are consistent with near-steady state production of N_2O from NO_3^-, although we must assume no kinetic isotope effect for NO_3^- reduction to N_2O. If N_2O is not held in steady state, then isotopic fractionation during NO_3^- reduction to N_2O could be accommodated, although additional N_2O consumption would be required due to the high observed $\delta^{15}N^{\alpha}$. This will be discussed in greater detail below.

A steady-state analysis was also conducted for $\delta^{15}N^{\beta}$, using the measured $\delta^{15}N_{NO2}$ (Fig. 8B gray boxes) and $\delta^{15}N_{NO3}$ (Fig. 8B, red boxes). Here, we also applied no kinetic isotope effect for NO_3^- or NO_2^- reduction to N_2O, but allowed an isotope effect of 2.2‰ for $\delta^{15}N^{\beta}$ fractionation during N_2O consumption (Ostrom et al., 2007). Measured $\delta^{15}N^{\beta}$ ranged from -20–0‰ (Fig. 8B, blue boxes), falling between the estimates for N_2O production from NO_3^- (Fig. 8B, red lines) and NO_2^- (Fig. 8B, gray lines). This indicates that either a mixture of sources contributes to $\delta^{15}N^{\beta}$, or that some isotopic fractionation is expressed during NO_3^- reduction to N_2O-β (though not between NO_3^- and N_2O-α). While equivalent fractionation between NO_3^- and N_2O-α and N_2O-β is generally assumed for denitrification (leading to low site preference), unequal fractionation has been observed in cultures of a denitrifying bacterium where NO_3^- was the substrate (Toyoda et al., 2005). A site preference has also been proposed to characterize N_2O production from a symmetrical intermediate during denitrification (Schmidt et al., 2004).

Measurements of $\delta^{18}O$ in NO_2^- and N_2O provide additional insight into the cycling of N_2O in the ODZ. $\delta^{18}O_{NO2}$ (Fig. 8C, gray boxes) and $\delta^{18}O_{NO3}$ (Fig. 8C, red boxes) provide

560 relatively uniform source values for N_2O produced via denitrification, though the isotope effects
561 between NO_3^- and N_2O differ markedly from those between NO_2^- and N_2O (Casciotti et al.,
562 2007). NO_2^- reduction via denitrification has a kinetic oxygen isotope effect of 2–6‰ (Martin
563 and Casciotti, 2016), and a branching isotope effect of 11–12‰ (Casciotti et al., 2007). If we
564 again assume no kinetic isotope effect during NO_2^- reduction but allow branching, N_2O produced
565 from NO_2^- via denitrification at our stations in the ETSP ODZ should have a maximum $\delta^{18}O_{N2O}$
566 value near 25‰ ($\delta^{18}O_{NO2}$ + 12‰). If N_2O consumption rates match those of production to
567 maintain N_2O in low steady state concentrations, N_2O consumption via denitrification with a
568 maximum isotope effect of 30‰ (Yamagishi et al., 2007) should leave the steady state $\delta^{18}O_{N2O}$
569 sourced from NO_2^- near 55‰ (Fig. 8C, gray lines). Instead, we observe $\delta^{18}O_{N2O}$ values of
570 80–100‰ (Fig. 8C, blue boxes), again suggesting that N_2O is not in isotopic steady state with
571 respect to a source from ambient NO_2^-. If we instead consider a source from NO_3^- (Fig. 8C, red
572 boxes), the expected $\delta^{18}O_{N2O}$ at steady state is 80–90‰ (Fig. 8C, red lines), due to the enhanced
573 fractionation between NO_3^- and N_2O (Casciotti et al., 2002; Toyoda et al., 2005; Casciotti et al.,
574 2007). Thus, N_2O derived from NO_3^- at steady state is consistent with the observed $\delta^{18}O_{N2O}$
575 values in the ODZ if no kinetic isotope effect for NO_3^- reduction is expressed.
576 Bourbonnais et al., (2017) found that $\delta^{15}N^{\beta}$ in the coastal Peruvian ODZ was also
577 depleted in ^{15}N, and used correlations between $\delta^{15}N^{bulk}$ and $\delta^{15}N_{NO3}$ and $\delta^{15}N_{NO2}$ to conclude that
578 there were sources from these precursors at and above the oxycline. At low O_2 concentrations,
579 the sources were less clear; however, they concluded that the low $\delta^{15}N^{\beta}$ signaled a transition
580 from net N_2O consumption to net N_2O production, and their model supported N_2O production
581 via denitrification in the lowest oxygen waters. Using N isotope tracer experiments, Ji et
582 al.,(2015) showed that both NO_3^- and NO_2^- contributed to N_2O production in the ETSP ODZ,

583 although NO_3^- appeared to contribute more than NO_2^-. Frame et al. (2017) also showed minimal
584 production of $^{15}N_2O$ from $^{15}NO_2^-$ in low oxygen waters off Namibia. From our analysis, a
585 mixture of N_2O production from NO_3^- and NO_2^- could explain the distributions of N isotope
586 signatures, although it is uncertain how NO_2^- would preferentially contribute to $\delta^{15}N^{\beta}$. A
587 plausible explanation of our isotopic data would be production of N_2O mostly from NO_3^-, with
588 enhanced fractionation between $\delta^{15}N_{NO3}$ and $\delta^{15}N^{\beta}$ compared with $\delta^{15}N^{\alpha}$. Such production of
589 N_2O with a site preference via denitrification of NO_3^- is not generally assumed, but could be
590 explained with preferential breakage of the bond between the N^{β} and its O atom in the symmetric
591 intermediate preceding N_2O formation from NO (Schmidt et al., 2004).
592 If ambient NO_2^- is a relatively minor substrate for N_2O production in the offshore ODZ, it
593 implies that production from NO_3^- occurs without complete exchange of the intermediate NO_2^-
594 with the external pool. This could occur if the denitrifying microbes that produce N_2O maintain
595 an internal pool of NO_2^- that is isotopically distinct from the external NO_2^- pool, or if
596 denitrification occurs on particles, where diffusion limitation restricts exchange of NO_2^- with the
597 ambient pool of NO_2^- and prevents expression of the kinetic isotope effects associated with NO_3^-
598 and NO_2^- reduction (Fuchsman et al., 2017). Both of these scenarios have been invoked to
599 explain the distributions of biogenic $\delta^{15}N_{N2}$, which in the ETSP is depleted in ^{15}N relative to
600 NO_2^- in the upper ODZ and enriched in ^{15}N relative to NO_2^- in the lower ODZ (Peters et al.,
601 2018). Without denitrification from an internal pool of NO_2^-, it is difficult to explain biogenic N_2
602 with a higher $\delta^{15}N$ than NO_2^-. Likewise, De Brabandere et al., (2014) suggested a similar
603 mechanism to explain the underestimation of denitrification from $^{15}NO_2^-$ incubations. They
604 argued that the $^{15}N/^{14}N$ of the NO_2^- that is denitrified may be lower than the external NO_2^- pool,

605 which would occur if $^{14}NO_3^-$ was also taken up and reduced to N_2 without full exchange of the
606 intracellular NO_2^- with the external pool.

607 Limited consumption of external NO_2^- via denitrification may also be consistent with a
608 dominant signal of NO_2^- oxidation in ambient NO_2^- in the offshore ETSP ODZ (Casciotti et al.,
609 2013; Gaye et al., 2013; Bourbonnais et al., 2015). In contrast, NO_2^- reduction appears more
610 influential in ambient NO_2^- signals in eddies and coastal ODZs where enhanced DIN
611 consumption has taken place (Bourbonnais et al., 2015; Hu et al., 2016). Perhaps in these
612 regions, where NO_3^- consumption is nearly complete, denitrifying bacteria are more likely to
613 access the external NO_2^- pool for their N_2O and N_2 production, explaining a more significant
614 relationship between $\delta^{15}N_{NO3}$, $\delta^{15}N_{NO2}$, $\delta^{15}N^{\alpha}$ and $\delta^{15}N^{\beta}$ at low oxygen concentrations in coastal
615 stations (Bourbonnais et al., 2017).

616

617 **5. Conclusion**

618 Investigations of N_2O concentration, isotopic and isotopomer data have allowed for
619 insights into the mechanisms of N_2O production and consumption in the ETSP, above, within,
620 and below the ODZ. Keeling plot analysis identified N_2O production in the surface and oxycline
621 layers as a mix of nitrifier denitrification and denitrification with some potential overprinting by
622 N_2O reduction during denitrification. For the deep layer, nitrification was more prominent with
623 some contribution from nitrifier-denitrification. The elevated values of $\delta^{15}N^{bulk}$, $\delta^{18}O_{N2O}$ and SP
624 for N_2O in the ODZ core are consistent with the occurrence of N_2O consumption. However,
625 evaluation of the relationship between $\delta^{18}O_{N2O}$ and SP in the ODZ identified a deviation from the
626 expected 2.2 slope expected for N_2O reduction alone (Ostrom et al., 2007). Regional water mass
627 mixing, varying isotope effects for N_2O reduction at different concentrations and N_2O production

628 in the ODZ via nitrification were evaluated and discounted as key drivers in this relationship.
629 While varying isotope effects (ε) were observed between different N_2O concentrations, we
630 believe this is a symptom rather than a cause of the deviation. Further evaluation reveals that the
631 elevated SP, relative to $\delta^{18}O_{N2O}$, at high extents of N_2O consumption could be attributed to the
632 shift towards more depleted $\delta^{15}N^{\beta}$ values in the ODZ core, maintaining high SP independent of
633 changes in $\delta^{15}N^{\alpha}$ and $\delta^{18}O_{N2O}$. The more depleted $\delta^{15}N^{\beta}$ signal is reflective of either enhanced
634 fractionation between NO_3^- and $\delta^{15}N^{\beta}$ relative to $\delta^{15}N^{\alpha}$ (denitrification with a site preference), or
635 preferential incorporation of a ^{15}N-depleted substrate, such as NO_2^-, into the N_2O-β position.
636 Overall, our analysis suggests that NO_3^- is an important source of N_2O in the offshore ETSP
637 ODZ, explaining much of the variation in $\delta^{15}N^{\alpha}$ and $\delta^{18}O_{N2O}$.
638
639 **6. Acknowledgments**
640 We thank the chief scientists, Professors Bess Ward and Alan Devol, for the opportunity to
641 collect samples on their cruise and their tireless support of ODZ N cycle research. We thank the
642 captain and crew of the R/V Nathaniel B. Palmer for their professional assistance at sea. We also
643 thank Bonnie Chang for helpful discussions during the early parts of data analysis. We thank
644 SCOR Working Group 144 for the opportunity to present and discuss these data in a workshop
645 on Microbial Responses to Ocean Deoxygenation in Goa, India. We also thank the NSF
646 Chemical Oceanography division for their support through grants 1140404 and 1233339 to KLC,
647 and grant 1233425 to CWM. Finally, we thank the reviewers for their constructive comments,
648 which greatly improved the manuscript. This publication was also partly funded by the Joint
649 Institute for the Study of the Atmosphere and Ocean (JISAO) under NOAA Cooperative

650 Agreements NA17RJ1232 and NA10OAR4320148, and is contribution 2017-084 to JISAO and
651 contribution 4663 to NOAA's Pacific Marine Environmental Laboratory.

References

1. Altabet M., 1988. Variations in nitrogen isotopic composition between sinking and suspended particles: implications for nitrogen cycling and particle transformation in the open ocean. Deep Sea Research I. 35: 535-554.
2. Arévalo-Martínez D.L., Kock. A., Löscher C.R., Scmidtz R.A., Bange H.W., 2015. Massive nitrous oxide emissions from the tropical south Pacific Ocean. Nature Geosc. 8, 530-533.
3. Babbin A.R., Bianchi D., Jayakumar A., Ward B.B., 2015. Rapid nitrous oxide cycling in the suboxic ocean. Science 348 6239, 1127-1129.
4. Babbin A.R., Peters B.D., Mordy C.W., Widner B., Casciotti K.L., Ward B.B., 2017. Multiple metabolisms constrain the anaerobic nitrite budget in the Eastern Tropical South Pacific. Global Biogeochemical Cycles 31: 258-271.
5. Bange H.W., Rapsomanikis S., Andreae M.O., 1996. Nitrous oxide emissions from the Arabian Sea. Geophy Res. Lett. 23(22).
6. Bange H.W., 2008. Gaseous nitrogen compounds (NO, N_2O, N_2, NH_3) in the ocean. In D.G. Capone, D.A. Bronk, M.R. Mulholland, and E.J. Carpenter (eds) *Nitrogen in the Marine Environment*. Pp. 51-94.
7. Bange H., Freing A., Kock A., Löscher C., 2010. Marine pathways to nitrous oxide. In *Nitrous Oxide and Climate Change*. pp. 36-62.
8. Beman J.M., Chow C.E., King A.L., Feng Y., Fuhrman A., Andersson A., Bates N.R., Popp B.N., Hutchins D.A., 2011. Global declines in ocean nitrification rates as a consequence of ocean acidification. Proceedings of National Academy of Sciences U.S.A. 108, 208-213.
9. Berelson W.M., Haskell W.Z., Prokopenko M., Knapp A.N., Hammond D.E., Rollins N., Capone D.G., 2015. Biogenic particle flux and benthic remineralization in the Eastern Tropical South Pacific. Deep-Sea Research I. 99: 23-34.
10. Bourbonnais A., Altabet M.A., Charoenpong C.N., Larkum J., Hu, H., Bange H.W., Stramma L., 2015. N-loss isotope effects in the Peru oxygen minimum zone studied using a mesoscale eddy as a natural tracer experiment. Global Biogeochemical Cycles. 29, 793-811.
11. Bourbonnais A., Letscher R.T., Bange H.W., Echevin V., Larkum J., Mohn J., Yoshida N., and Altabet, M.A., 2017. N_2O production and consumption from stable isotopic and concentration data in the Peruvian coastal upwelling system. Global Biogeochemical Cycles. 31, 678-698.
12. Bryan B.A., Shearer G., Skeeters J.L., Kohl D.H., 1983. Variable expression of nitrogen isotope effect associated with denitrification of nitrite. Journal of Biological Chemistry. 258, 8613-8617.
13. Carrasco C., Karstensen J., Farias L., 2017. On the nitrous oxide accumulation in intermediate waters of the Eastern South Pacific Ocean. Frontiers in Marine Science. 4: 24.
14. Casciotti K.L., Sigman D.M., Hastings MG., Böhlke J.K., Hilkert A., 2002. Measurement of the oxygen isotopic composition of nitrate in seawater and freshwater using the denitrifier method. Anal. Chem. 74(19), 4905-4912.
15. Casciotti K.L., Böhlke J.K., McIlvin M.R., Mroczkowski S.J., Hannon J.E., 2007. Oxygen isotope in nitrite: analysis, calibration and equilibration. Anal. Chem. 79, 2427-2436.
16. Casciotti K.L., McIlvin M.R., 2007. Isotopic analyses of nitrate and nitrite from reference mixtures and application to Eastern Tropical North Pacific waters. Marine Chemistry. 107, 184-201.

17. Casciotti K.L., Buchwald, C. Insights on the marine microbial nitrogen cycle from isotopic approaches to nitrification. Frontiers in Microbiology. 3, 356.
18. Casciotti K.L., Buchwald C., McIlvin M., 2013. Implications of nitrate and nitrite isotopic measurements for the mechanisms of nitrogen cycling in Peru oxygen deficient zone. Deep. Sea. Res. I. 80, 78-93.
19. Ciais P., Sabine C., Bala G., Bopp L., Brovkin V., Canadell J., Chhabra A., DeFries R., Galloway J., Heimann M., Jones C., Le Quéré C., Myneni R.B., Piao S., Thornton P., 2013. Carbon and Other Biogeochemical Cycles. In: *Climate Change 2013: The Physical Science Basis. Contribution of Working Group I to the Fifth Assessment Report of the Intergovernmental Panel on Climate Change* [Stocker, T.F., D. Qin, G.-K. Plattner, M. Tignor, S.K. Allen, J. Boschung, A. Nauels, Y. Xia, V. Bex and P.M. Midgley (eds.)]. Cambridge University Press, Cambridge, United Kingdom and New York, NY, USA.
20. Codispoti L.A., Christensen J.P., 1985. Nitrification, denitrification and nitrous oxide cycling in the eastern tropic south Pacific Ocean. Mar. Chem. 16, 277-300.
21. Codispoti L.A., 2010. Interesting times for marine N_2O. Science. 327, 1339-1340.
22. Crutzen P.J., 1970. The influence of nitrogen oxides on the atmospheric ozone content. Q.J.R. Meterol. Soc. 96, 320-325.
23. Czeschel R., Stramma L., Schwarzkopf F.U., Giese B.S., Funk A., Karstensen J., 2011. Middepth circulation of the eastern tropical South Pacific and its link to the oxygen minimum zone. Journal of Geophysical Research 116, C01015.
24. Deutsch C., Gruber N., Key R.M., Sarmiento J.L., Ganaschaud A., 2001. Denitrification and N_2 fixation in the Pacific Ocean. Glo. Biogeo. Cyc. 15(2):483-506.
25. De Brabandere L., Canfield D.E., Dalsgaard T., Friederich G.E., Revsbech N.P., Ulloa O., Thamdrup B., 2014. Vertical partitioning of nitrogen-loss processes across the oxic-anoxic interface of an oceanic oxygen minimum zone. Environmental Microbiology. 16, 3041-3054.
26. De Pol-Holz R., Robinson R.S., Hebbeln D., Sigman D.M., Ulloa O., 2009. Controls on sedimentary nitrogen isotopes along the Chile margin. Deep-Sea Res. II, 56, 1042-1054.
27. Dore J.E., Popp B.N., Karl D.M., Sansome F.J., 1998. A large source of nitrous oxide from subtropical North Pacific surface waters. Nature 396, 63-66.
28. Farias L., Paulmier A., Gallegos M., 2007. Nitrous oxide and N-nutrient cycling in the oxygen minimum zone off northern Chile. Deep Sea Res I. 54, 164-180
29. Farias L., Castro-Gonzalez M., Cornejo M., Charpentier J., Faundez J., Boontanon N., Yoshida N., 2009. Denitrification and nitrous oxide cycling within the upper oxycline of the eastern tropical South Pacific oxygen minimum zone. Limnol. Oceanog. 54(1) 132-144.
30. Frame C.H., Casciotti K.L., 2010. Biogeochemical controls and isotopic signatures of nitrous oxide production by a marine ammonia-oxidizing bacterium. Biogeo. 7, 2695-2709.
31. Frame C.H., Lau E., Nolan J., Goepfert T.J., Lehmann M.F., 2017. Acidification enhances hybrid N_2O production associated with aquatic ammonia-oxidizing microorganisms. Frontiers in Microbiology. 7, 2104.
32. Freing A.D., Wallace W.R., Bange H.W., 2012. Global oceanic production of nitrous oxide, Philos. Trans. R. Soc. B, 367, 1157–1168.
33. Fuchsman C.A., Devol A.H., Casciotti K.L., Buchwald C., Chang B.X., Horak R.E.A., 2017. An N isotope mass balance of the Eastern Tropical North Pacific oxygen deficient zone. Deep Sea Research II. doi. 10.1016/j.dsr2.201.12.013.
34. Fujii A., Toyoda S., Yoshida O., Watanabe S., Sasaki K., Yoshida N., 2013. Distribution of nitrous oxide dissolved in water masses in the eastern subtropical North Pacific and its origin

742 inferred from isotopomer analysis. J. Ocean. 69, 147-157.
743 35. Garcia-Robledo E., Borisov S., Klimant I., Revsbech N.P., 2016. Determination of
744 respiration rates in water with sub-micromolar oxygen concentrations. Frontiers in Marine
745 Science. 3, 244.
746 36. Gordon, L. I., J. C. Jennings Jr, A. A. Ross, and J. M. Krest (1993), A suggested protocol for
747 continuous flow automated analysis of seawater nutrients (phosphate, nitrate, nitrite and
748 silicic acid) in the WOCE Hydrographic Program and the Joint Global Ocean Fluxes Study,
749 Methods Manual WHPO 91–1, WHP Operations and Methods, WOCE Hydrographic
750 Program Office, La Jolla, Calif.
751 37. Goreau T.J., Kaplan W.A., Wofsy S.C., McElroy M.B., Valois F.W., Watson S.W. 1980.
752 Production of NO_2 and N_2O by nitrifying bacteria at reduced concentration of oxygen. Appl.
753 Environ. Microbiol. 40(3) 526-532.
754 38. Granger J., Sigman D.M., 2009. Removal of nitrite with sulfamic acid for nitrite N and O
755 isotope analysis with the denitrifier method. Rap. Comm. Mass. Spec. 23, 3753-3762.
756 39. Grasse P., Ehlert C. Frank M., 2013. The influence of water mass mixing on the dissolved Si
757 isotope composition of the Eastern Equatorial Pacific. Earth and Planetary Science Letters
758 380: 60-71.
759 40. Gruber N, Sarmiento J.L., 1997. Global patterns of marine nitrogen fixation and
760 denitrification. Glob. Biogeochem. Cyc. 11(2):235-266.
761 41. Hu H., Bourbonnais A., Larkum J., Bange H.W., Altabet M.A., 2016. Nitrogen cycling in
762 shallow low-oxygen coastal waters off Peru from nitrite and nitrate nitrogen and oxygen
763 isotopes. Biogeosciences. 13, 1453-1468.
764 42. Ji Q., Babbin A.R., Jayakumar A., Oleynik S., Ward B.B., 2015. Nitrous oxide production by
765 nitrification and denitrification in the Eastern Tropical South Pacific oxygen minimum zone.
766 Geophysical Research Letters 42: 10755-10764.
767 43. Jinuntuya-Nortman M., Sutka R.L., Ostrom P.H., Gandhi H., Ostrom N.E., 2008.
768 Isotopologue fractionation during microbial reduction of N_2O within soil mesocosms as a
769 function of water-filled pore space. Soil Biology and Biogeochemistry. 40, 2273-2280.
770 44. Karstensen J., Tomczak M., 1998. Age determination of mixed water masses using CFC and
771 oxygen data. J. Geophys. Res. 103: 18,599 – 18,609.
772 45. Keeling C.D., 1961. The concentration and isotopic abundance of carbon dioxide in rural and
773 marine air. Geochimica et Cosmochimica Acta 24: 277-298.
774 46. Kim J.R., Craig H., 1993. Nitrogen-15 and oxygen-18 characteristics of nitrous oxide: A
775 global perspective. Science. 262, 1855:1857.
776 47. Kock A., Arévalo-Martínez D.L., Löscher C.R., Bange H.W., 2016. Extreme N_2O
777 accumulation in the coastal oxygen minimum zone off Peru. Biogeosciences. 13, 827-840.
778 48. Kozlowski J.A., Stieglmeier M., Schleper C., Klotz M.G., Stein L.Y., 2016. Pathways and
779 key intermediates required for obligate aerobic ammonia-dependent chemolithotrophy in
780 bacteria and Thaumarchaeota. ISME Journal 10: 1836-1845.
781 49. Langdon, C., 2010. Determination of dissolved oxygen in seawater by Winkler titration using
782 the amperometric technique. The GOSHIP Repeat Hydrography Manual: a Collection of
783 Expert Reports and Guidelines, edited by: Hood, EM, Sabine, CL, and Sloyan, BM.
784 50. Lewicka-Szczebak et al., 2017.
785 51. Llanillo P.J., Karstensen J., Pelear J.L., Stramma L., 2013. Physical and biogeochemical
786 forcing of oxygen and nitrate changes during El Nino/ El Viejo and La Nina/ La Vieja upper-
787 ocean phases in the tropical eastern South Pacific along 86W. Biogeosci. 10, 6339-6355.

52. Lipschultz F., Wofsy S.C., Ward B.B., Codispoti L.A., Friedrich G., Elkins J.W., 1990. Bacterial transformations of inorganic nitrogen in the oxygen-deficient waters of the Eastern Tropical South Pacific Ocean. Deep. Sea. Res. Pt A, 37, 1513-1541
53. Löscher C.R., Kock A., Könneke M., LaRoche J., Bange H.W., Schmitz R.A., 2012. Production of oceanic nitrous oxide by ammonia-oxidizing archaea. Biogeosciences. 9, 2419-2429.
54. Mackas D.L., Denman K.L., Bennett A.F., 1987. Least Squares Multiple Tracer Analysis of Water Mass Composition. J. Geophys. Res. 92, 2907 – 2918.
55. Mariotti A., Germon J.C., Hubert P., Kaiser P., Letolle R., Tardieux A., Tardieux P., 1981. Experimental determination of nitrogen kinetic isotope fractionation: some principles; illustration for the denitrification and nitrification processes. Plant and Soil. 62, 413-430.
56. Martin T.S., Casciotti K.L., 2016. Nitrogen and oxygen isotopic fractionation during microbial nitrite reduction. Limnol. Oceanog. 61, 1134-1143.
57. Martinez-Rey J., Bopp L., Gehlen M., Tagliabue A., Gruber N., 2015. Projections of oceanic N_2O emissions in the 21st Century using the IPSL Earth System Model. Biogeosci. 12, 4133-4148.
58. McIlvin M.R., Casciotti, K.L. 2010. Fully automated system for stable isotopic analyses of dissolved nitrous oxide at natural abundance levels. Limnology and Oceanography: Methods. 8, 54-66.
59. McIlvin M.R., Casciotti K.L., 2011. Technical updates to the bacterial method for nitrate isotopic analyses. Anal. Chem. 83, 1850-1856.
60. Mohn J., Wolf B., Toyoda S., Lin C-T., Liang M-C., Bruggemann N., Wissel H., Steiker A.E., Dyckmans J., Szwec L., Ostrom N.E., Casciotti K.L., Forbes M., Giesesmann A., Well R., Doucett R.R., Yarnes C.T., Ridley A.R., Kaiser J., Yoshida N., 2014. Interlaboratory assessment of nitrous oxide isotopomer analysis by isotope ratio mass spectrometry and laser spectroscopy: current status and perspectives. Rap. Comm. Mass. Spec. 28, 1995-2007.
61. Montoya J.P., Carpenter E.J., Capone D.G., 2002. Nitrogen fixation and nitrogen isotope abundances in zooplankton of the oligotrophic North Atlantic. Limnology and Oceanography. 47, 1617-1628.
62. Myhre G., Shindell D., Bréon F.-M., Collins W., Fuglestvedt J., Huang J., Koch D., Lamarque J.-F., Lee D., Mendoza B., Nakajima T., Robock A., Stephens G., Takemura T., Zhang H., 2013. Anthropogenic and natural radiative forcing. In: *Climate Change 2013: The Physical Science Basis. Contribution of Working Group I to the Fifth Assessment Report of the Intergovernmental Panel on Climate Change*. Stocker T.F., Qin D., Plattner G.-K., Tignor M., Allen S.K., Boschung J., Nauels A., Xia Y., Bex V., Midgley P.M. (eds). Cambridge University Press, New York, NY, USA, pp. 659-740.
63. Naqvi S.W.A., Bange H.W., Farias L., Montreio P.M.S., Scranton M.I., Zhang I., 2010. Marine hypoxia/anoxia as a source of CH_4 and N_2O. Biogeosci. 7, 2159-2190.
64. Naqvi S.W.A., Noronha R.J., 1991. Nitrous oxide in the Arabian Sea. Deep-Sea Res. 38, 871-890.
65. Nevison C.D., Butler J.H., Elkins J.W., 2003. Global distribution of N_2O and the ΔN_2O-AOU yield in the subsurface ocean. Glo. Biogeochem. Cyc. 17, 4, 1119
66. Nevison C.D., Lueker T.J., Weiss R.F., 2004. Quantifying the nitrous oxide source from coastal upwelling. Glo. Biogeochem. Cyc. 18, GB1018, 1-17

67. Nicholls J.C., Davies C.A., Trimmer N., 2007. High-resolution profiles and Nitrogen isotope tracing reveal a dominant source of nitrous oxide and dominant pathways of nitrogen gas formation in the central Arabian Sea. Limnol. Oceanog. 52, 156-169.
68. Ostrom N.E., Russ M.E., Popp B., Rust T.M., Karl D.M., 2000. Mechanisms of nitrous oxide production in the subtropical North Pacific based on determinations of the isotopic abundances of nitrous oxide and di-oxygen. Chemosphere—Global Change Science. 2, 281-290.
69. Ostrom N.E., Pitt A., Sutka R., Ostrom P.H., Grandy A.S., Huizinga K.M., Robertson G.P., 2007. Isotopologue effects during N_2O reduction in soils and in pure cultures of denitrifiers. J. Geophys. Res. 112 G02005, 1-12.
70. Ostrom N.E., Ostrom P.H., 2012. The isotopomers of nitrous oxide: Analytical considerations and application to resolution of microbial production pathways. In *Handbook of Environmental Isotope Geochemistry*, Advances in Isotope Geochemistry. Baskaran, M. (ed.), pp. 453-476.
71. Pataki D.E., Ehleringer J.R., Flanagan L.B., Yakir D., Bowling D.R., Still C.J., Buchmann N., Kaplan J.O., Berry J.A., 2003. The application and interpretation of Keeling plots in terrestrial carbon cycle research. Global Biogeochemical Cycles 17: 1022.
72. Peters B., Casciotti K.L., Horak R., Devol A.H., Fuchsman C., Forbes M., Mordy C., 2018. Estimating fixed nitrogen loss and associated isotope effects using concentration and isotope measurements of NO_3^-, NO_2^-, and N_2 from the Eastern Tropical South Pacific oxygen deficient zone. Deep Sea Research II. doi: 10.1016/j.dsr2.2018.02.011.
73. Peters B.D, Babbin A.R., Lettmann K.A., Mordy C.W., Ulloa O., Ward B.B., Casciotti K.L., 2016. Vertical modeling of the nitrogen cycle in the eastern tropical South Pacific oxygen deficient zone using high-resolution concentration and isotope measurements. Global Biogeochemical Cycles 30: 1661-1681.
74. Popp B., Westley N., Toyoda S., Miwa T., Dore J., Yoshida N., Rust T., Sansome F., Russ M., Ostrom N., Ostrom P., 2002. Nitrogen and oxygen isotopomeric constraints on the origins and sea-to-air flux of N_2O in the oligotrophic subtropical North Pacific gyre. Glo. Biogeochem. Cyc. 16, 1064.
75. Rahn T., Wahlen M., 2000. A reassessment of the global isotopic budget of atmospheric nitrous oxide. Glo. Biogeochem. Cyc. 14, 537-543.
76. Ravishankara A.R., Daniel J.S., Portmann R.W., 2009. Nitrous Oxide (N_2O): The dominant ozone-depleting substance emitted in the 21st century. Science. 326, 123-125.
77. Revsbech N.P., Larsen L.H., Gundersen J., Dalsgaard T., Ulloa O., Thamdrup B., 2009. Determination of ultra-low oxygen concentrations in oxygen minimum zones by the STOX sensor. Limnology and Oceanography: Methods. 7, 371-381.
78. Santoro A.E., Buchwald C., McIlvan M.R., Casciotti K.L., 2011. Isotopic signature of N_2O produced by Marine Ammonia Oxidizing Archea. Science. 333, 1282-1285.
79. Sigman D.M., Casciotti K.L., Andreani M., Barford C., Galanter M., Bohlke J.K., 2001. A bacterial method for the nitrogen isotopic analysis of nitrate in seawater and freshwater. Anal. Chem. 73, 4145-4153.
80. Silva N., Rojas N., Fedele A., 2009. Water masses in the Humboldt Current System: Properties, distribution, and the nitrate deficit as a chemical water mass tracer for Equatorial Subsurface Water of Chile. Deep-Sea Research II 56: 1004-1020.
81. Schlitzer R., 2000. Ocean-Data-View, http://www.awi-bremerhaven.de/GEO/ODV.

82. Schmidt H.-L., Werner R.A., Yoshida N., Well R., 2004. Is the isotopic composition of nitrous oxide an indicator for its origin from nitrification or denitrification? A theoretical approach from referred data and microbiological and enzyme kinetic aspects. Rapid Communications in Mass Spectrometry 18: 2036-2040.
83. Snider D.M., Venkiteswaran J.J., Schiff S.L., Spoelstra J., 2012. Deciphering the oxygen isotope composition of nitrous oxide produced by nitrification. Global Change Biology. 18, 356-370.
84. Stein L.Y., Yung Y.L., 2003. Production, isotopic composition, and atmospheric fate of biologically produced nitrous oxide. Annual Reviews of Earth and Planetary Science. 31, 329-356.
85. Stieglmeier M., Mooshammer M., Kitzler B., Wanek W., Zechmeister-Boltenstern S., Richter A., Schleper C., 2014. Aerobic nitrous oxide production through N-nitrosating hybrid formation in numerous oxidizing bacteria. ISME J. 8(5), 1135-1146
86. Stramma L., Johnson G.C., Sprintall J., Mohrholz V., 2008. Expanding oxygen-minimum zones in the tropical oceans. Science. 320, 655-658.
87. Suntharalingam P., Sarimento J.L., 2000. Factors governing the oceanic nitrous oxide distribution: simulations with an ocean general circulation model. Glo. Biogeochem. Cyc. 14, 429-454.
88. Sukta R.L. Ostrom N.E., Ostrom P., Gandhi H., Breznak J., 2003. Nitrogen isotopomer site preference of N_2O produced by *Nitrosomonas europaea* and *Methylococcus capsulatus* Bath. Rap. Comm. Mass. Spec. 17, 738-745.
89. Sukta R.L. Ostrom N.E., Ostrom P., Gandhi H., Breznak J., 2004. Nitrogen isotopomer site preference of N_2O produced by *Nitrosomonas europaea* and *Methylococcus capsulatus* Bath. Rap. Comm. Mass. Spec. 18, 1411-1412.
90. Sutka R.L., Ostrom N.E., Ostrom P.H., Breznak J.A., Gandhi H., Pitt A.J., Li F., 2006. Distinguishing nitrous oxide production from nitrification and denitrification on the basis of isotopomer abundances. App. Environ. Microbiol. 72 638-644.
91. Thamdrup B., Dalsgaard, T., Revsbech N.P., 2012. Widespread functional anoxia in the oxygen minimum zone of the eastern South Pacific. Deep-Sea Research I. 65, 36-45.
92. Tiano L., Garcia-Robledo E., Dalsgaard T., Devol A.H., Ward B.B., Canfield D.E., Revsbech N.P., 2014. Oxygen distribution and aerobic respiration in the north and south eastern tropical Pacific oxygen minimum zones. Deep-Sea Research I. 94, 173-183.
93. Tomczak M., Large D.G.B., 1989. Optimum Multiparameter Analysis of Mixing in the Thermocline of Eastern Indian Ocean. J. Geophys. Res. 94, 16,141 – 16,149.
94. Toyoda S., Yoshida N., 1999. Determination of nitrogen isotopomers of nitrous oxide on a modified isotope mass spectrometer. Anal. Chem. 71(20), 4711-4718.
95. Toyoda S., Yoshida N., Miwa T., Matsui Y., Yamagishi H., Tsunogai U., Nojiri Y., Tsurushima N., 2002. Production mechanism and global budget of N_2O inferred from its isotopomers in the western North Pacific. Geophys. Res. Lett. 29(3), 1037.
96. Toyoda S., Mutobe H., Yamagishi H., Yoshida N., Tanji Y., 2005. Fractionation of N_2O isotopomers during production by denitrifier. Soil. Biol. Biochem. 37, 1535-1545.
97. Trimmer M., Chronopoulou P.-M., Maanoja S.T., Upstill-Goddard R.C., Kitidis V., Purdy K.J., 2016. Nitrous oxide as a function of oxygen and archael gene abundance in the North Pacific. Nature Communications. 7, 13451.

98. Webster E.A., Hopkins D.W., 1996. Nitrogen and oxygen isotope ratios of nitrous oxide emitted from soil and produced by nitrifying and denitrifying bacteria. Biol. Fertil. Soils. 22, 326-330.
99. Weiss R.F., Price B.A., 1980. Nitrous oxide solubility in water and seawater. Mar. Chem. 8, 347-359.
100. Westley M.B., Yamagishi H., Popp B.N., Yoshida N., 2006. Nitrous oxide cycling in the Black Sea inferred from stable isotope and isotopomer distributions. Deep-Sea Res. II. 53, 1802-1816.
101. Westley M.B., Popp B.N., Rust T.M., 2007. The calibration of the intra molecular nitrogen isotope distribution in nitrous oxide measured by isotope ratio mass spectrometry. Rap. Comm. Mass. Spec. 21(3), 391-405.
102. Wrage N., Velthof, G.L., van Beusichem M.L., Oenema O., 2001. Role of nitrifier denitrification in the production of nitrous oxide. Soil Biology and Biochemistry. 33, 1723-1732.
103. Wright J.J., Konwar K.M., Hallam S.J., 2012. Microbial ecology of expanding Oxygen minimum zones. Nat. Rev. Microbiol. 10, 381-394.
104. Yamagishi H., Yoshida S., Toyoda B., Popp N., Westley M.B., Watanabe S., 2005. Contributions of denitrification and mixing on the distribution of nitrous oxide in the North Pacific. Geophys. Res. Lett. 32, L04603.
105. Yamagishi H., Westley M.B., Popp B.N., Toyoda S., Yoshida N., Watanabe S., Koba K., Yamanaka Y., 2007. Role of nitrification and denitrification on the nitrous oxide cycle in the eastern tropical North Pacific and Gulf of California. J. Geophys. Res. 112, 1-15.
106. Yoshida N., Hattori A., Saino T., Matsuo S., Wada E. 1984. $^{15}N/^{14}N$ ratio of dissolved N_2O in the eastern tropical Pacific Ocean. Nature. 307, 442-444.
107. Yoshida N., 1988. ^{15}N-depleted N_2O as a product of nitrification. Nature. 335 (6190), 528-529.
108. Yoshida N., Toyoda S., 2000. Constraining the atmospheric N_2O budget from intramolecular site preference in N_2O isotopomers. Nature. 405, 330-334.
109. Zamora L.M., Oschlies A., Bange H.W., Huebert K.B., Craig J.D., Kock A., Löscher C.R., 2012. Nitrous oxide dynamics in low oxygen regions of the Pacific: insights from the MEMENTO database. Biogeosciences. 9, 5007-5022.

952 **Table 1**: Estimated isotopic composition of N_2O sources

Layer	$\delta^{15}N^{bulk}$ (‰ vs. atm N_2)	$\delta^{18}O_{N2O}$ (‰ vs. VSMOW)	Site Preference (‰)
Surface	6.2 ± 1.3‰	51.9 ± 3.0‰	6.8 ± 4.3‰
Oxycline	7.6 ± 2.2‰	50.9 ± 3.4‰	9.4 ± 2.5‰
Deep	6.6 ± 0.6‰	54.2 ± 0.6‰	20.2 ± 0.6‰

953

954 **Table 2**: Apparent isotope effects for N_2O consumption in the ODZ

	Upper ODZ	Middle ODZ	Lower ODZ	Ostrom et al., 2007
$\varepsilon^{18}O$	25.6 ± 6.5‰	19.6 ± 4.5‰	14.5 ± 3.4‰	10.9-15.0‰
εSP	17.5 ± 5.5‰	21.8 ± 3.1‰	11.6 ± 2.9‰	5.0-6.8‰
$\varepsilon^{18}O/\varepsilon SP$	1.46 ± 0.56	0.90 ± 0.36	1.25 ± 0.45	2.2

955

Figure Legends

Figure 1. Cruise track for ETSP 2013 cruise (NBP-1305) of the coasts of Peru and Chile, with stations discussed in this study labeled and highlighted by fringing circles. Plotted in Ocean Data View (Schlitzer, 2000).

Figure 2. Depth profiles of (A) oxygen (μM), (B) nitrite (μM), and (C) nitrous oxide (nM) for the seven stations measured during the NBP-1305 cruise in 2013.

Figure 3. Depth profiles of (A) $\delta^{15}N^{bulk}$, (B) $\delta^{18}O$, (C) site preference (SP), (D) $\delta^{15}N^{\alpha}$, and (E) $\delta^{15}N^{\beta}$ of nitrous oxide (N_2O) for the seven stations measured during the NBP-1305 cruise in 2013.

Figure 4. Keeling plot analysis of N_2O sources for surface (filled circles), oxycline (filled triangles), and deep (open circles) layers. Linear regressions of $\delta^{15}N^{bulk}$ (A), $\delta^{18}O_{N2O}$ (B), and N_2O site preference (C) vs. $1/[N_2O]$ are shown with solid lines and 95% confidence intervals on the regressions are shown for each series (dashed lines).

Figure 5. $\delta^{18}O_{N2O}$ vs. $\delta^{15}N^{\alpha}$ (A) and $\delta^{18}O_{N2O}$ vs. SP (B), for the ETSP ODZ samples ($26.2 \leq \sigma_\theta \leq 26.8$ kg m^{-3}). In (A), the solid line represents the expected $\delta^{15}N^{\alpha}$ vs. $\delta^{18}O_{N2O}$ relationship for N_2O consumption via denitrification (Ostrom et al., 2007). In (B), the solid lines reprenset the expected slopes of SP vs. $\delta^{18}O_{N2O}$ during denitrification from two hypothesized source waters: Eastern South Pacific Intermediate Water (ESPIW, left) and Equatorial Subsurface Water (ESSW, right). Mixing between the two water masses is represented by the dashed arrow.

Figure 6. Apparent isotope effects for $\delta^{18}O_{N2O}$ ($\varepsilon^{18}O$) and site preference (εSP) during N_2O consumption in the ETSP ODZ, with data separated into upper ODZ (gray symbols), middle ODZ (black symbols), and lower ODZ (white symbols). Isotope effects were obtained using a Rayleigh equation from the slopes of $\delta^{18}O_{N2O}$ (A) or SP (B) vs. $-\ln([N_2O])$, where $[N_2O]$ is the concentration of dissolved N_2O in nmol/L. εSP was highest in the middle ODZ, while $\varepsilon^{18}O$ was highest in the upper ODZ. These patterns led to the lowest ratio of $\varepsilon^{18}O/\varepsilon SP$ in the middle ODZ, relative to that expected from denitrification (Ostrom et al., 2007; Jinuntuya-Nortman et al., 2008).

Figure 7. $\delta^{15}N^{\alpha}$, $\delta^{15}N^{\beta}$, SP, $\delta^{18}O_{N2O}$, $\delta^{15}N_{NO3}$ and $\delta^{15}N_{NO2}$ as a function of depth for stations BB1 (A), 5 (B), 17 (C), and 18 (D). The shaded portion of each panel represents the ODZ, with upper middle, and lower ODZ layers separated by dashed and dot-dashed lines, respectively. Clearly evident at each station is a depletion in $\delta^{15}N^{\beta}$ and an increase in SP in the middle ODZ. $\delta^{15}N^{\alpha}$ and $\delta^{18}O_{N2O}$ closely tracked each other, while SP exhibits a decoupling from $\delta^{15}N^{\alpha}$ and $\delta^{18}O_{N2O}$ in the middle ODZ due to the lowered $\delta^{15}N^{\beta}$.

Figure 8. Box and whisker plots of observed $\delta^{15}N^{\alpha}$ (A), $\delta^{15}N^{\beta}$ (B), and $\delta^{18}O_{N2O}$ (C) relative to observed $\delta^{15}N_{NO2}$ and $\delta^{15}N_{NO3}$, or $\delta^{18}O_{NO3}$ and $\delta^{18}O_{NO2}$, as well as calculated steady state $\delta^{15}N^{\alpha}$, $\delta^{15}N^{\beta}$, and $\delta^{18}O_{N2O}$. Observed N_2O data are given in blue boxes, while observed NO_3^- and NO_2^- data are given in red and gray boxes, respectively. The boxes show the range of 25 to 75th percentile of ODZ observations at each station, with the median value for each station shown with a horizontal line inside each box. Error bars show 90th and 10th percentiles for

measurements of ODZ N_2O and NO_2^-. The calculated steady-state □□□□values from NO_3^- and NO_2^- are given by the red and gray lines, respectively, with the 50th percentile shown with the solid lines and the 25th and 75th percentiles shown with the dashed lines in each panel.

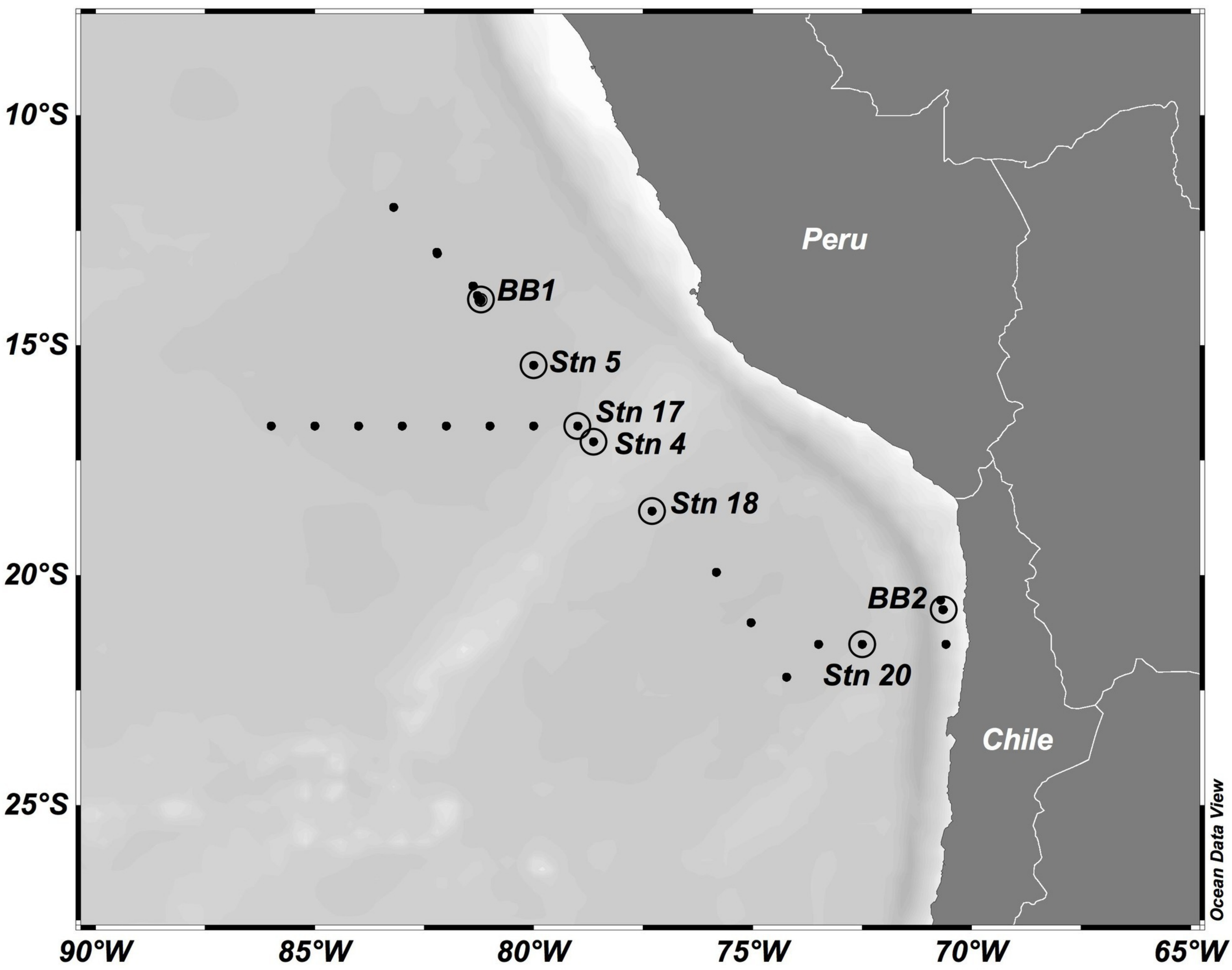
10°S
15°S
20°S
25°S
90°W
85°W
80°W
75°W
70°W
65°W
Peru
Chile
BB1
Stn 5
Stn 17
Stn 4
Stn 18
BB2
Stn 20
Ocean Data View

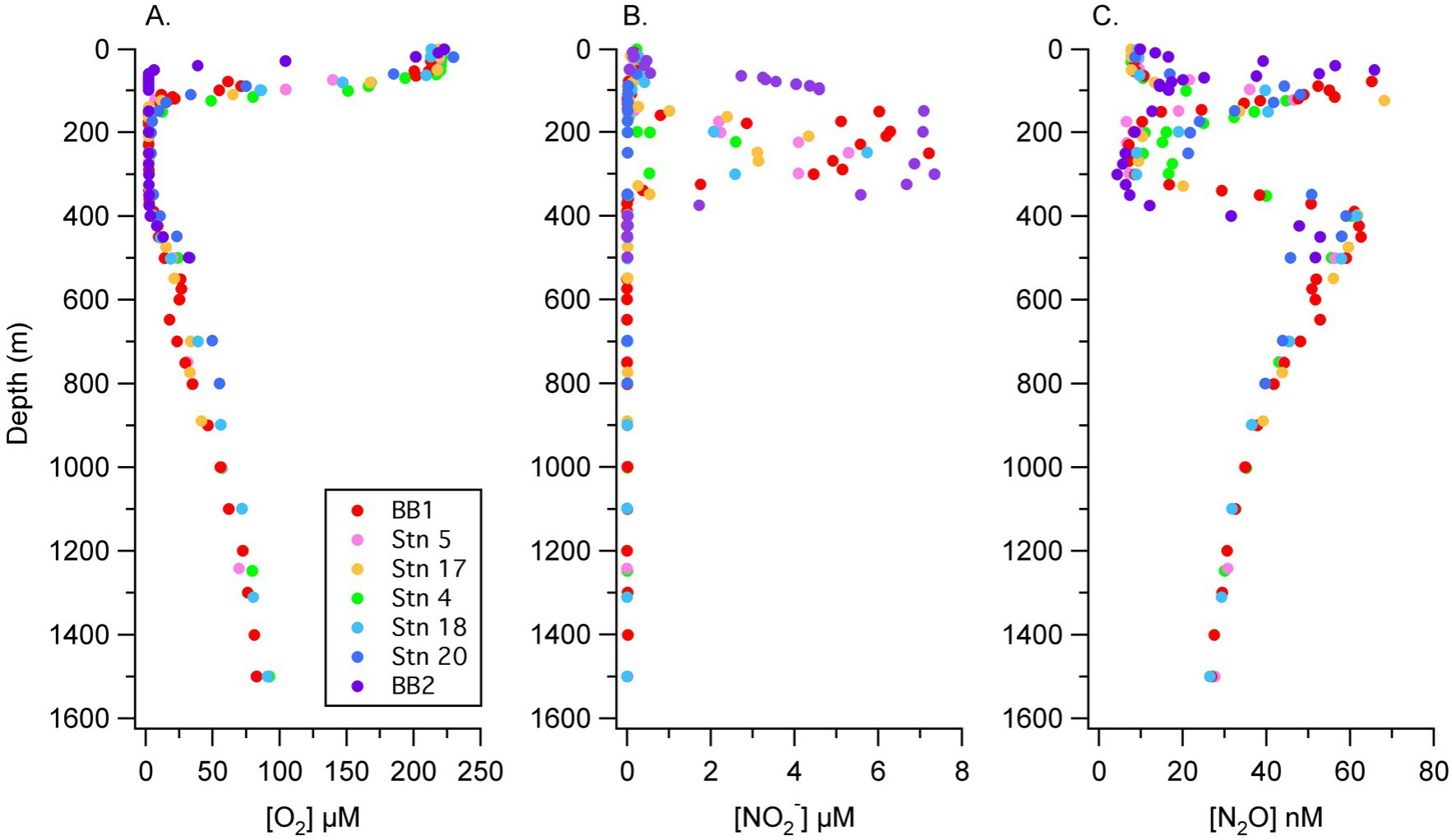
A.
B.
C.
Depth (m)
0
200
400
600
800
1000
1200
1400
1600
0
50
100
150
200
250
[O2] µM
0
2
4
6
8
[NO2-] µM
0
20
40
60
80
[N2O] nM
BB1
Stn 5
Stn 17
Stn 4
Stn 18
Stn 20
BB2

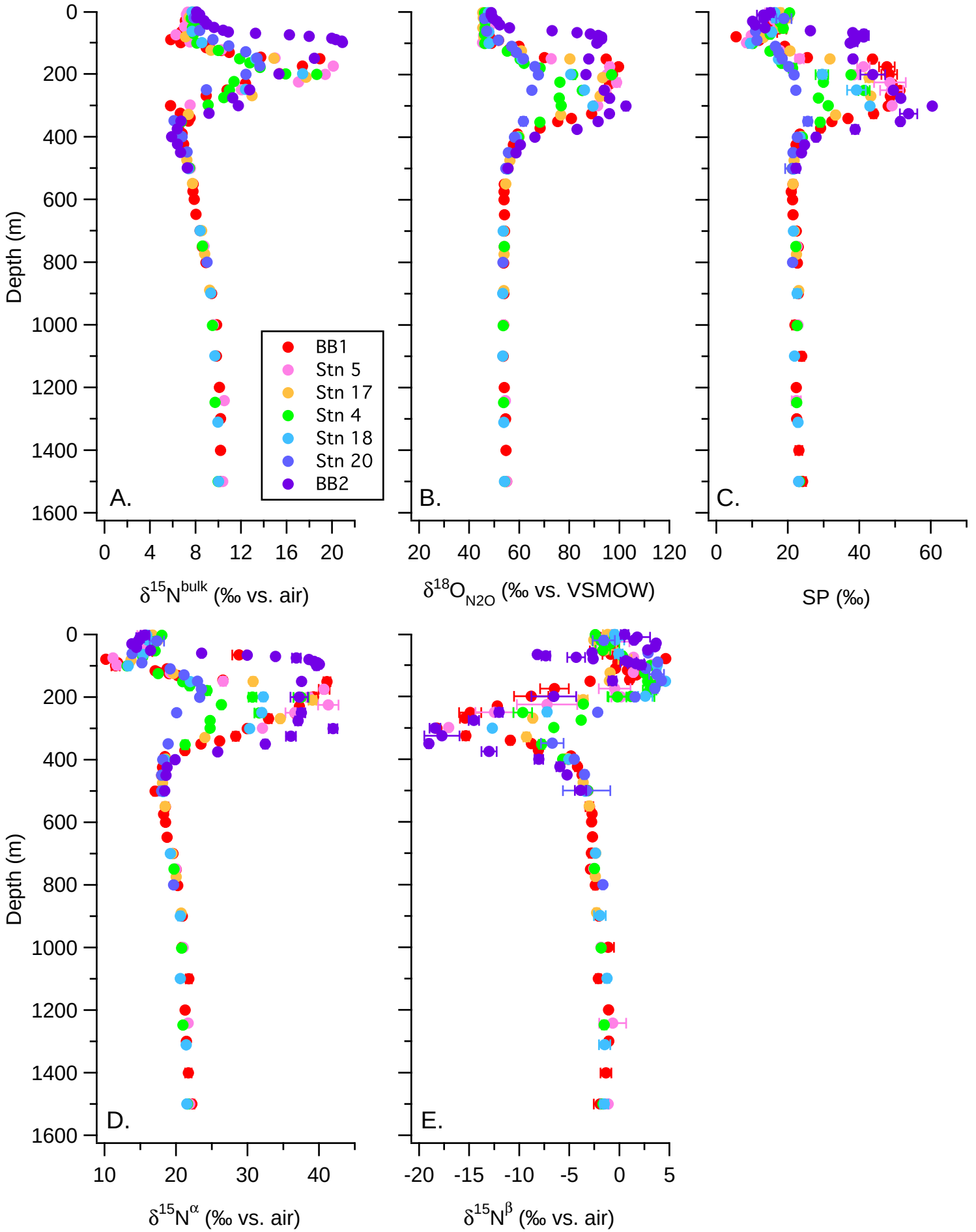
Depth (m)
0
200
400
600
800
1000
1200
1400
1600
A.
0
4
8
12
16
20
δ15Nbulk (‰ vs. air)
BB1
Stn 5
Stn 17
Stn 4
Stn 18
Stn 20
BB2
B.
20
40
60
80
100
120
δ18ON2O (‰ vs. VSMOW)
C.
0
20
40
60
SP (‰)
D.
10
20
30
40
δ15Nα (‰ vs. air)
E.
-20
-15
-10
-5
0
5
δ15Nβ (‰ vs. air)

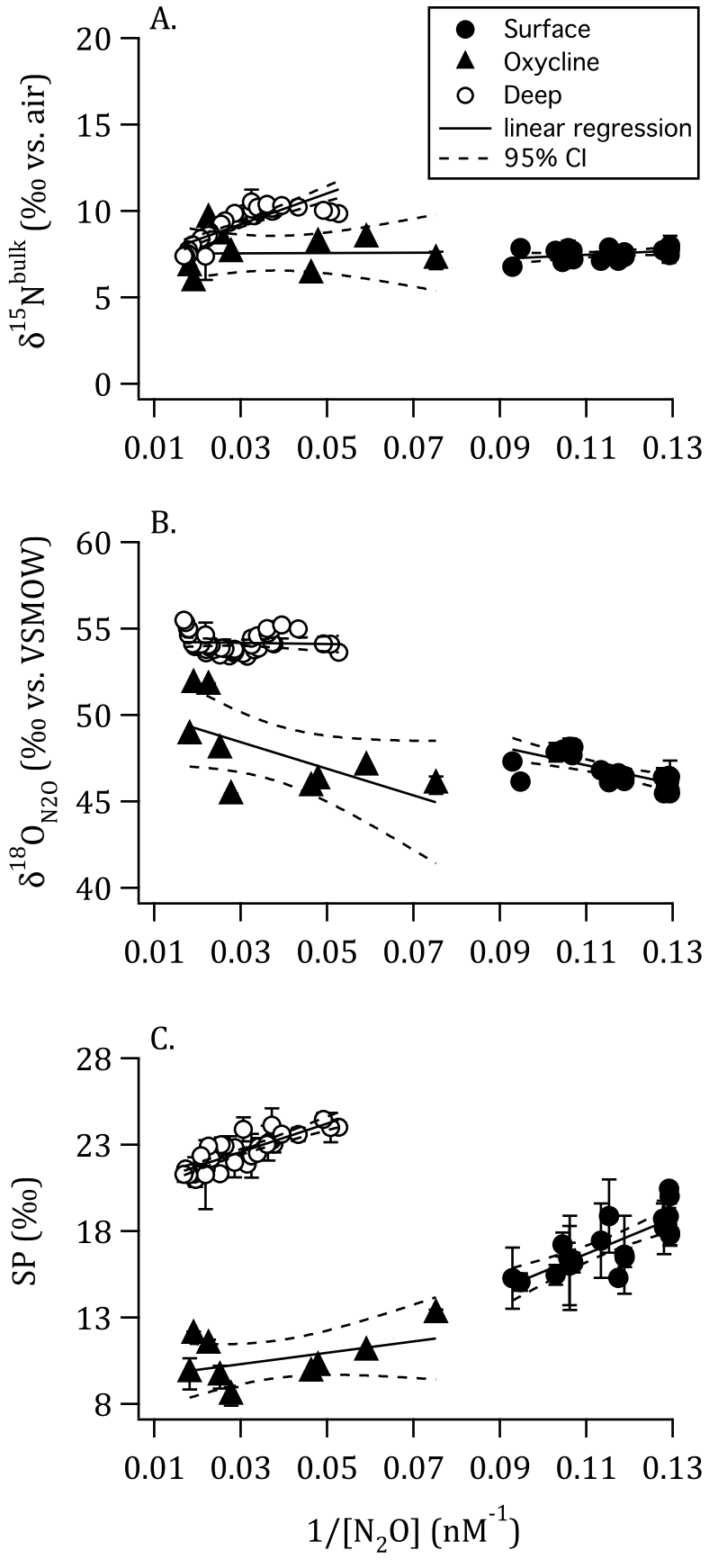
A.
Surface
Oxycline
Deep
linear regression
95% CI
$\delta^{15}N^{bulk}$ (‰ vs. air)
20
15
10
5
0
B.
$\delta^{18}O_{N2O}$ (‰ vs. VSMOW)
60
55
50
45
40
C.
SP (‰)
28
23
18
13
8
0.01
0.03
0.05
0.07
0.09
0.11
0.13
$1/[N_2O]$ (nM^{-1})

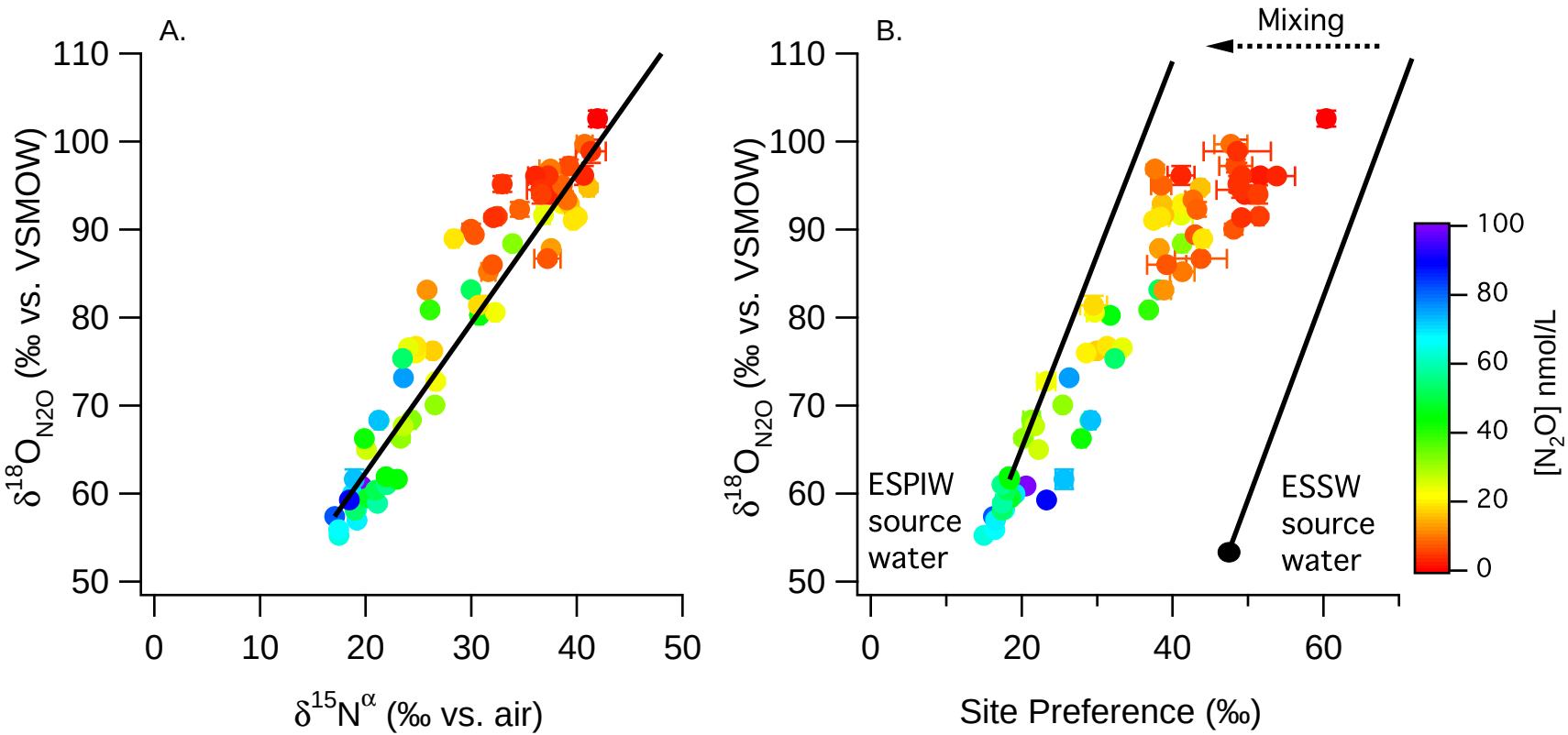
A.
B.
Mixing
ESPIW source water
ESSW source water
δ18ON2O (‰ vs. VSMOW)
δ15Nα (‰ vs. air)
Site Preference (‰)
[N2O] nmol/L
110
100
90
80
70
60
50
0
10
20
30
40
50
60
100
80
60
40
20
0

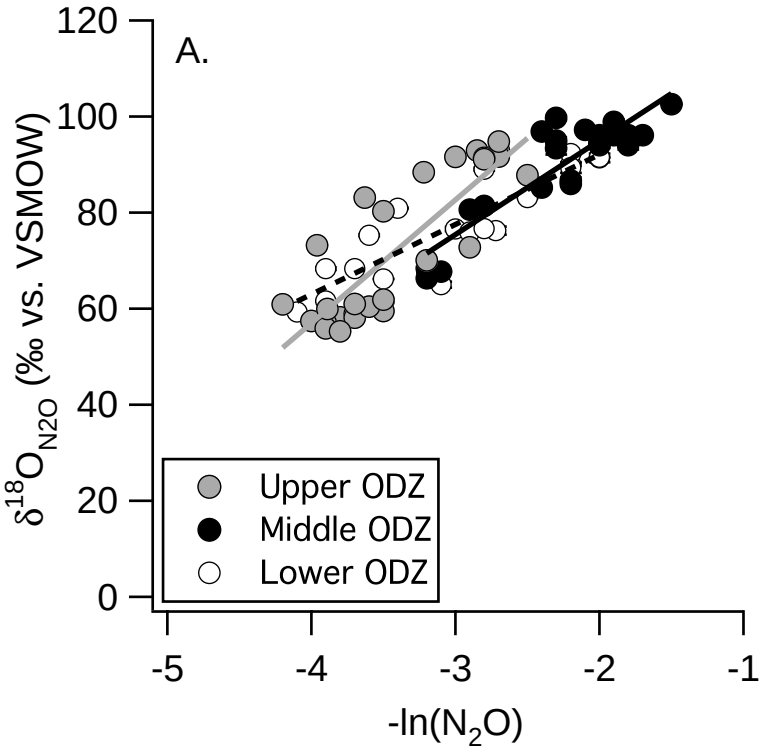
A.
120
100
80
60
40
20
0
-5
-4
-3
-2
-1
δ18ON2O (‰ vs. VSMOW)
-ln(N2O)
Upper ODZ
Middle ODZ
Lower ODZ

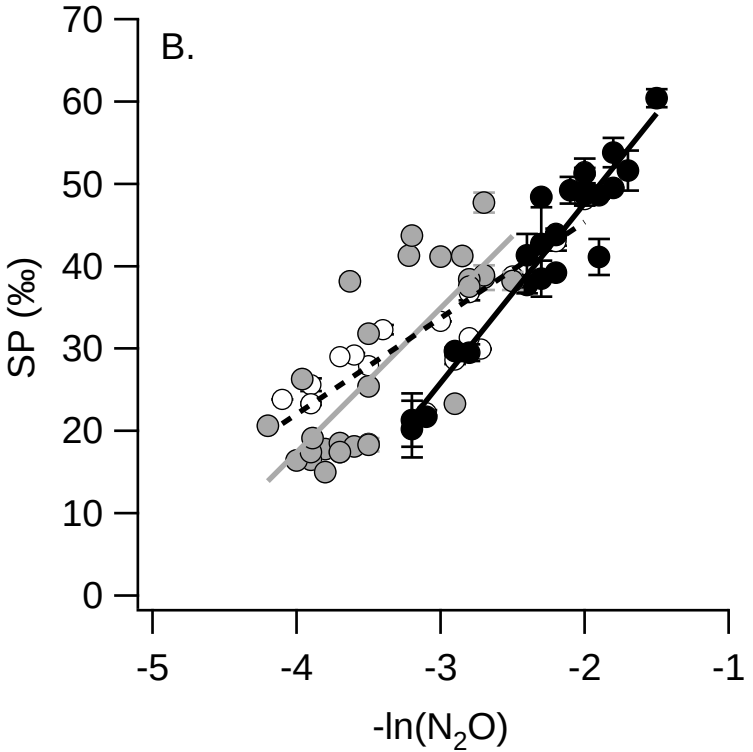
B.
70
60
50
40
30
20
10
0
-5
-4
-3
-2
-1
SP (‰)
-ln(N2O)

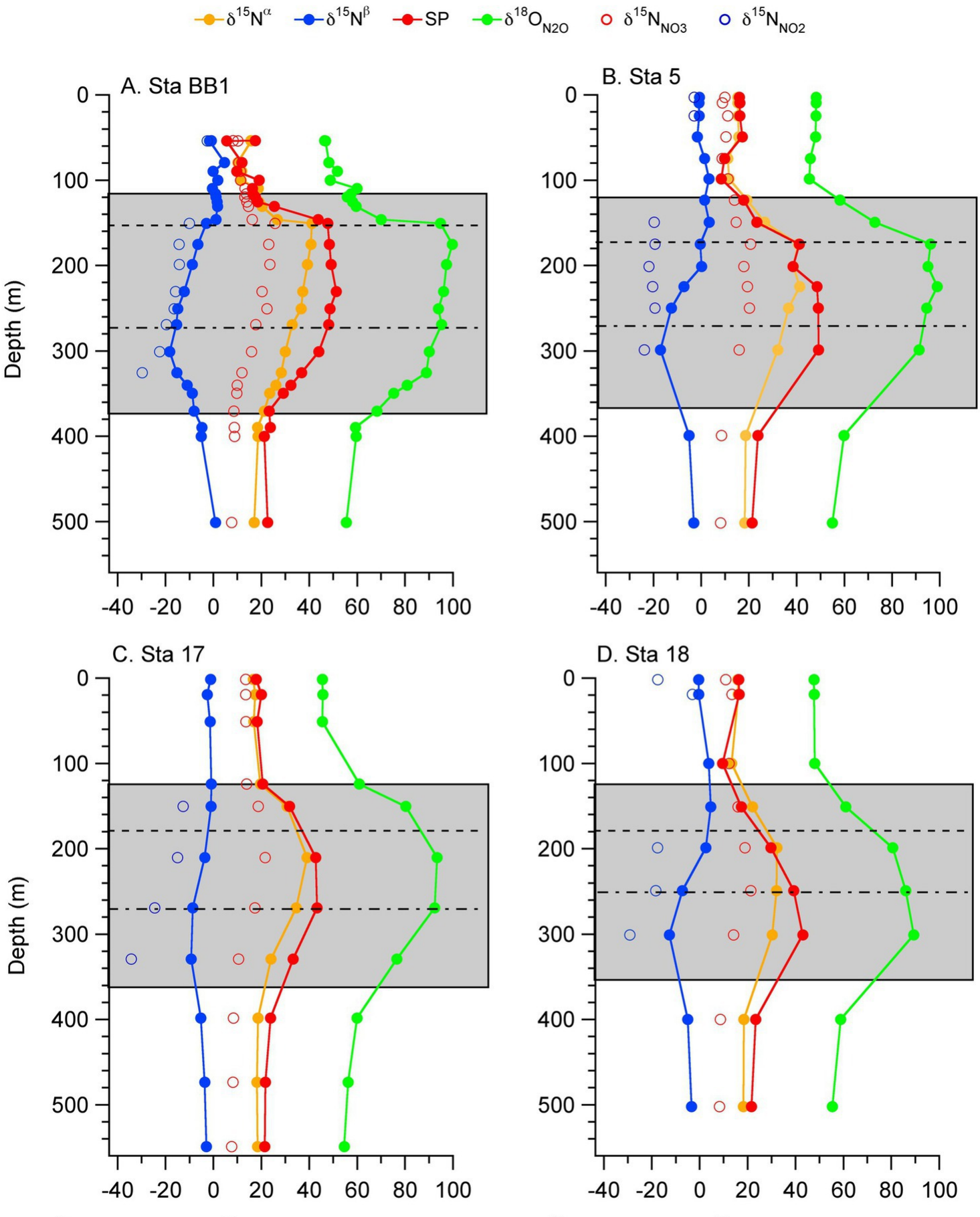
δ15Nα
δ15Nβ
SP
δ18ON2O
δ15NNO3
δ15NNO2
A. Sta BB1
B. Sta 5
C. Sta 17
D. Sta 18
Depth (m)
0
100
200
300
400
500
-40
-20
0
20
40
60
80
100
δ15N (‰ vs. air), δ18O (‰ vs. VSMOW), and SP
δ15N (‰ vs. air), δ18O (‰ vs. VSMOW), and SP

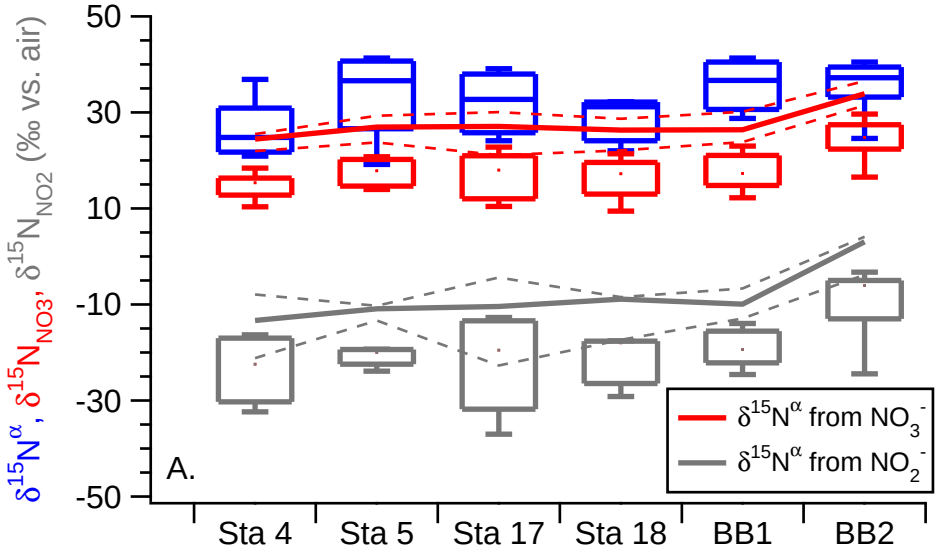
50
30
10
-10
-30
-50
A.
δ15Nα from NO3-
δ15Nα from NO2-
Sta 4
Sta 5
Sta 17
Sta 18
BB1
BB2
δ15Nα, δ15NNO3, δ15NNO2 (‰ vs. air)

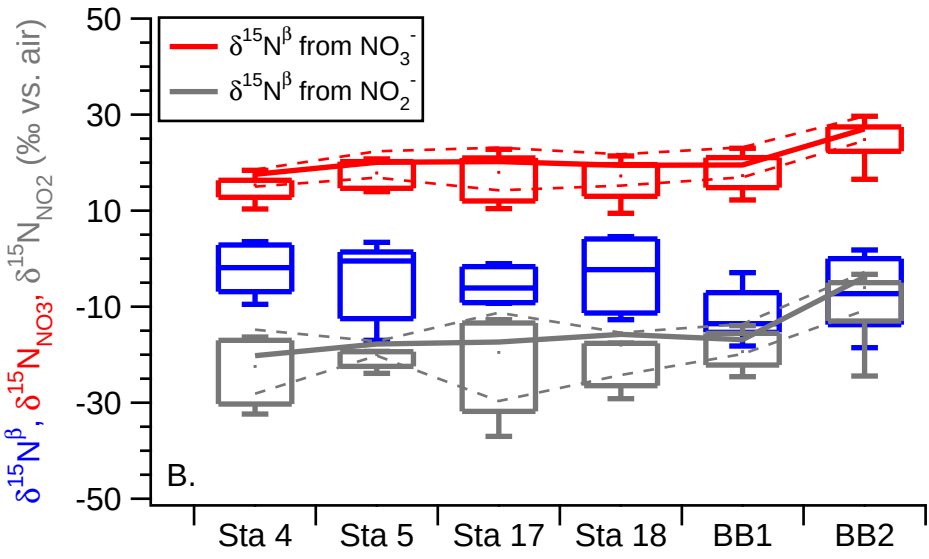
50
30
10
-10
-30
-50
B.
δ15Nβ from NO3-
δ15Nβ from NO2-
Sta 4
Sta 5
Sta 17
Sta 18
BB1
BB2
δ15Nβ, δ15NNO3, δ15NNO2 (‰ vs. air)

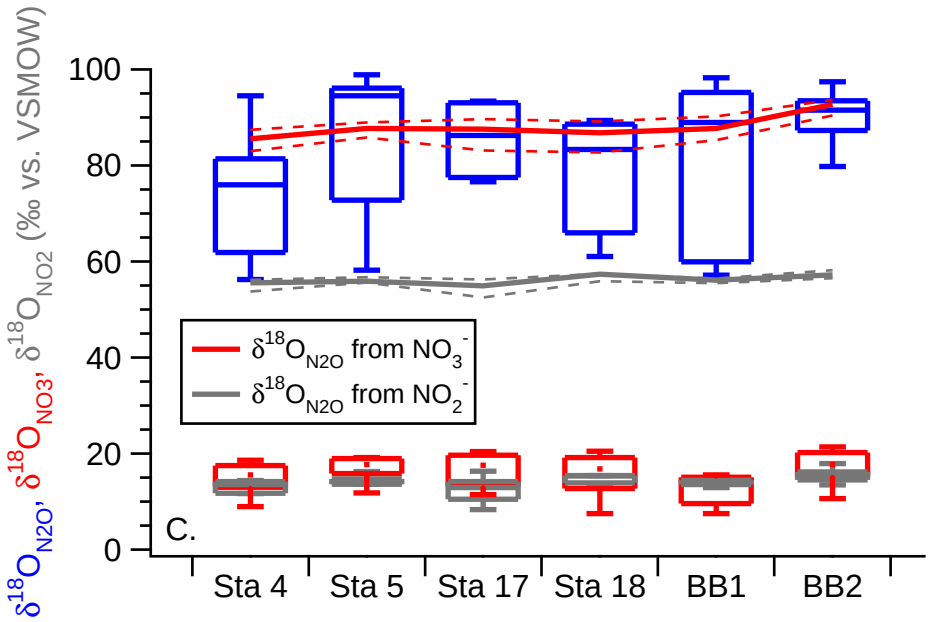
100
80
60
40
20
0
C.
δ18ON2O from NO3-
δ18ON2O from NO2-
Sta 4
Sta 5
Sta 17
Sta 18
BB1
BB2
δ18ON2O, δ18ONO3, δ18ONO2 (‰ vs. VSMOW)